



HAL
open science

A single master regulator controls asexual cell cycle division patterns in *Toxoplasma gondii*

Asma S. Khelifa, Cecilia Sanchez Guillen, Kevin M. Lesage, Ludovic Huot, Pierre Péricard, Nicolas Barois, Hélène Touzet, Guillemette Marot, Mathieu Gissot

► **To cite this version:**

Asma S. Khelifa, Cecilia Sanchez Guillen, Kevin M. Lesage, Ludovic Huot, Pierre Péricard, et al.. A single master regulator controls asexual cell cycle division patterns in *Toxoplasma gondii*. 2020. hal-03107529v1

HAL Id: hal-03107529

<https://hal.science/hal-03107529v1>

Preprint submitted on 24 Nov 2020 (v1), last revised 12 Jan 2021 (v2)

HAL is a multi-disciplinary open access archive for the deposit and dissemination of scientific research documents, whether they are published or not. The documents may come from teaching and research institutions in France or abroad, or from public or private research centers.

L'archive ouverte pluridisciplinaire **HAL**, est destinée au dépôt et à la diffusion de documents scientifiques de niveau recherche, publiés ou non, émanant des établissements d'enseignement et de recherche français ou étrangers, des laboratoires publics ou privés.



Distributed under a Creative Commons Attribution - NonCommercial - NoDerivatives 4.0 International License

A single master regulator controls asexual cell cycle division patterns in *Toxoplasma gondii*

Asma S. Khelifa ¹, Cecilia Sanchez Guillen ¹, Kevin M. Lesage ¹, Ludovic Huot ¹, Pierre Pericard ², Nicolas Barois ¹, Helene Touzet ^{2,3}, Guillemette Marot ^{2,4} and Mathieu Gissot ^{1,*}.

1. Univ. Lille, CNRS, Inserm, CHU Lille, Institut Pasteur de Lille, U1019 - UMR 9017 - CIIL - Center for Infection and Immunity of Lille, F-59000 Lille, France.
2. Univ. Lille, CNRS, Inserm, CHU Lille, Institut Pasteur de Lille, US 41 - UMS 2014 - PLBS, bilille, F-59000 Lille, France.
3. Univ. Lille, CNRS, Centrale Lille, UMR 9189 - CRIStAL - Centre de Recherche en Informatique Signal et Automatique de Lille, F-59000 Lille, France.
4. Univ. Lille, Inria, CHU Lille, ULR 2694 - METRICS: Evaluation des technologies de santé et des pratiques médicales, F-59000 Lille, France.

* Corresponding author: mathieu.gissot@pasteur-lille.fr

ABSTRACT

All apicomplexan parasites have complex life cycles exhibiting division characterized by a tightly regulated cell cycle control, resulting in the emergence of daughter parasites in possession of a single nucleus and a complete set of organelles. Apicomplexa have evolved efficient and distinctive strategies for intracellular replication where the timing of emergence of the daughter cells, a process termed “budding”, is a decisive element. However, the molecular mechanisms that provide the proper timing of parasite budding remain unknown. Using *Toxoplasma gondii* as a model Apicomplexa, we identified a master regulator that controls the timing of the budding process. We show that an ApiAP2 transcription factor, TgAP2IX-5, controls cell cycle events downstream of centrosome duplication including organelle division and segregation. TgAP2IX-5 binds to the promoter of hundreds of genes and controls the activation of the budding-specific cell cycle expression program. We show that TgAP2IX-5 regulates the expression of specific transcription factors that are necessary for the completion of the budding cycle. TgAP2IX-5 acts as a licensing factor that ensures that asexual proliferation continues by promoting the inhibition of the differentiation pathway at each round of the cell cycle. Therefore, TgAP2IX-5 is a master regulator that controls both cell cycle and developmental pathways.

INTRODUCTION

Apicomplexa is a phylum consisting of unicellular, obligate, intracellular protozoan parasites of high transmissibility, which includes various human pathogen species such as *Plasmodium* spp. (causative agent of malaria), *Toxoplasma* spp. (cause of toxoplasmosis) and *Cryptosporidium* spp. (cause of cryptosporidiosis).

Apicomplexan parasites trigger disease associated with an uncontrollable expansion of parasite biomass resulting in inflammation and host cell destruction [1]. Although, apicomplexan parasites usually present a sexual cycle within the definitive host, the pathogenesis of these parasites results from the ongoing asexual replication cycles within the host's cells. All Apicomplexa have complex life cycles exhibiting a proliferation characterized by a tightly regulated cell cycle control and resulting in the emergence of daughter parasites with a single nucleus and a complete set of organelles [2]. Apicomplexa have evolved the ability to independently divide their nucleus (nuclear cycle) and produce the parasite body through a process that is termed budding (budding cycle). This allows flexibility in order to produce a suitable number of offspring in a single cell cycle while allowing the parasite to cope with the different host-cell environments [3]. Apicomplexa have evolved efficient and distinctive strategies for intracellular replication [1]. How the division pattern is chosen to ensure parasite expansion during host-cell infection remains unanswered. However, it has been clear that the mode of division is dependent on the timing and coordination of the nuclear and budding cycles [4,5].

Plasmodium falciparum and *Toxoplasma gondii* represent two modern branch points of the Apicomplexa phylum, a divergence that occurred several hundred million years ago [6]. This divergence has led to changes in the usage of different cell division patterns. For instance, in its intermediate host, *Plasmodium falciparum* replicates through schizogony, a division pattern

which produces a multinucleated intermediate (schizont) where the daughter parasites bud from the periphery at the closure of the division process to produce infective merozoites. By contrast, in its intermediate hosts, *Toxoplasma gondii* undergoes endodyogeny, a division pattern that consists of the formation of two daughter parasites within the mother cell. In this case, the formation of new daughter cells occurs within the cytoplasm rather than from the periphery [1] and is coordinated to arise simultaneously with nuclear division. In addition to endodyogeny, which is the simplest form of internal budding, *T. gondii* asexually divides within its definitive host through a division scheme that closely resembles schizogony. Endopolygeny consists of the production of multiple nuclei and a final step of daughter cell formation where parasites bud from the cytoplasm [7]. These three distinct replication patterns (endodyogeny, schizogony and endopolygeny) rely on the coordination of the timing of the budding and nuclear cycles. Apicomplexa, such as *T. gondii* which exhibit endodyogeny and endopolygeny, are able to employ several division patterns depending on the environment and host. Such a flexibility suggests overlapping mechanisms in control of the cell cycle independent of the division pattern used.

Apicomplexa show a peculiar cell cycle with a closed mitosis that is divided into three phases (G1, S and M) while the G2 phase is apparently absent [8]. Centrosomes play a central role in controlling the cell cycle in Apicomplexa. They serve as the microtubule organizing center (MTOC) for the mitotic spindle and are key to position the site of daughter cell assembly [5,9]. In *T. gondii*, the bipartite nature of the centrosome allows an independent control of both the nuclear and budding cycles [9]. Centrosome division happens between the end of G1 and the start of S phase [2] and marks the beginning of the budding cycle. Division and maturation of the centrosome controls the progression and the coordination of the nuclear and budding cycle [5,9–12]. Evidence suggests that soon after centrosome division, centrosome maturation

through kinases is key to the activation of daughter cell formation [9,11,12]. Cell cycle dependent expression of these kinases may be important to control their activity [11,12].

During the Apicomplexa cell cycle, division and segregation of organelles is a highly ordained process in order to ensure that each daughter parasite acquires the proper complement of organelles. During *T. gondii* endodyogeny, Golgi widening and replication is the first step to occur during the G1 phase [13]. This is followed by apicoplast duplication, endoplasmic reticulum division and is concluded with the division of the mitochondria [14]. Specialized secretory organelles such as the rhoptries and micronemes are generated de-novo in a process that begins after nuclear division [14]. This highly controlled process implies a tight regulation of the gene expression during the cell cycle. This was illustrated by the transcriptomic analysis of synchronous cell cycle populations indicating that *T. gondii* may have adapted a “just in time” mode of expression whereby transcripts and proteins are produced right when their function is needed [15]. This suggests that transcriptional regulation of gene expression may exert a centralized control on both centrosome activation and the expression of proteins needed for daughter cell formation.

However, little is known on the potential regulators that may control this transcriptional switch. Apicomplexan genomes encode a family of putative transcription factors that are characterized by the possession of one or more DNA binding AP2 domains [16]. ApiAP2 transcription factors were shown to control expression profiles during *T. gondii* differentiation [17–19]. ApiAP2s were also shown to cooperatively control the expression of virulence factors [20,21] in *T. gondii* indicating that this family of transcription factors may control cell cycle dependent expression profiles as also suggested for *P. berghei* [22]. In this study, we functionally characterize a cell cycle dependent ApiAP2 transcription factor, TgAP2IX-5. We show that it controls cell cycle events downstream of centrosome duplication including organelle division and segregation. TgAP2IX-5 binds to the promoter of hundreds of genes and

controls the activation of the S/M-specific cell cycle expression program. Reversible destabilization of the TgAP2IX-5 protein showed that its expression is sufficient for activation of the budding cycle in multinucleated parasites. Therefore, controlled TgAP2IX-5 expression allows for the switching from endodyogeny to endopolygeny division patterns. TgAP2IX-5 acts as a master regulator controlling the budding cycle and therefore, asexual cell cycle division patterns in this parasite.

RESULTS

TgAP2IX-5 is a cell-cycle regulated transcription factor essential for parasite growth and proliferation

To find specific regulators of the cell cycle dependent expression program, we identified potential transcriptional regulators whose expression was cell cycle regulated [15]. Among these regulators, we focused on the ApiAP2 family of transcription factors and discovered that the *tgap2ix-5* transcript was dynamically expressed with a peak of expression within the S phase (toxodb.org). To confirm that the TgAP2IX-5 protein was also cell cycle regulated, we produced a *T. gondii* strain that had an epitope-tagged version of this gene at its endogenous locus. Immuno-fluorescence assays using cell-cycle markers demonstrated that TgAP2IX-5 is a nuclear protein mostly expressed during the early S phase (Figure 1A). TgAP2IX-5 expression was detected at the G1/S transition and early S phase when centrosomes are divided but remained in close proximity of each other (as identified by TgCentrin1; a marker of the outer core of the centrosome, Figure 1A upper panel, Figure S1A). TgAP2IX-5 was detected before centromere division (as identified by TgChromol; a marker of pericentromeric chromatin [23], Figure 1A middle panel, Figure S1B-C) but not after (late S phase), indicating that TgAP2IX-5 was only present during the G1/S transition and early S phase. TgAP2IX-5 was no longer detected when parasites enter the S/M phase (as indicated by an early budding marker TgISP1, (Figure 1A, lower panel). Therefore, TgAP2IX-5 protein expression is tightly controlled during the cell cycle.

To identify the biological role of TgAP2IX-5, an inducible knock down (iKD) mutant of TgAP2IX-5 was generated using the AID system which allowed for the conditional depletion of the TgAP2IX-5 protein (Figure 1B). For this purpose, we produced a strain that presented an AID-HA insert at the 3' end of the TgAP2IX-5 gene using a CrispR/Cas9 strategy (Figure S2A). The correct locus of integration of this insert was confirmed by PCR (Figure S2B). The

AID system allows for the conditional depletion of the target protein after addition of auxin (indoleacetic acid) (Figure 1B). A single detectable band at the expected protein size (251 kDa) was present in absence of auxin in the iKD TgAP2IX-5 strain as verified by Western-Blot (Figure 1C). Rapid depletion of the TgAP2IX-5 protein (as early as 1 hour) was obtained in iKD TgAP2IX-5 mutant strain grown in media containing auxin (Figure 1C).

iKD TgAP2IX-5 mutant displays a defect in daughter parasite formation

To phenotypically characterize the iKD TgAP2IX-5 mutant, a standard growth assay was carried out. The growth capacity of the iKD TgAP2IX-5 mutant in the presence of auxin was tested and we observed that the iKD TgAP2IX-5 mutant growth ability was drastically decreased in the presence of auxin (Figure 2A). In fact, growth was completely abrogated in the iKD TgAP2IX-5 mutant in presence of auxin with a calculated mean of 1 parasite per vacuole while the parental strain (in presence and absence of auxin) and the iKD TgAP2IX-5 mutant in absence of auxin grew at a mean of 2.5 parasites per vacuole. This demonstrated a complete blockage of the proliferation capacity of the parasite in the absence of TgAP2IX-5 (Figure 2A). A plaque assay, that measured the ability of the parasite to grow and invade over a period of seven days confirmed the phenotype with the absence of lysis plaques in the iKD TgAP2IX-5 strain treated with auxin contrary to the control used (parental strain in presence of auxin) where lysis plaques were observed (Figure S3A). These results suggest that TgAP2IX-5 expression is essential for the parasite's growth and proliferation.

To better assess the growth phenotype, we examined the parasite by IFA using a nucleus marker (TgENO2) and an inner membrane complex (IMC) marker (TgIMC1), a network of flattened vesicles lying beneath the plasma membrane (Figure 2B). It was apparent that the parasite accumulated nuclei and did not form daughter cells in absence of TgAP2IX-5 while exhibiting normal daughter cell formation in presence of the protein. To confirm the inability of the

parasite to form daughter cells in presence of auxin, we performed transmission electron microscopy and observed that in absence of auxin the iKD TgAP2IX-5 mutant was able to produce daughter cells while in presence of auxin the parasite accumulated nuclei associated with lack of apparent daughter cell formation (Figure 2C). To confirm these observations, we measured the number of parasites per nuclei (Figure 2D and S3B-C). Depending on the timing during the cell cycle, the parasites exhibit either one nucleus (80 % of the total parasite population) or two nuclei (20 % of the total parasite population) (before or after cytokinesis) for the parental strain (in absence or in presence of auxin) and for the iKD TgAP2IX-5 strain in absence of auxin (Figure 2D and S3B-C). By contrast, the percentage of parasite exhibiting more than 2 nuclei increased overtime in the iKD TgAP2IX-5 strain in presence of auxin (Figure 2D and S3B-C). The observation of multi-nucleated parasites in presence of auxin suggests that the iKD TgAP2IX-5 mutant displays a defect in daughter parasite formation but not in the ability of the parasite to multiply and segregate its nuclear material. To assess the capacity of the iKD TgAP2IX-5 mutant to produce daughter cells, we recorded the number of parasite cells that were in the process of producing daughter cells through internal budding (Figure 2B and E and Figure S4A-B), therefore measuring the parasite's ability to produce daughter cells at an early stage of internal budding. Using two different markers, we were able to show a drastic decrease of the number of parasites undergoing budding in the iKD TgAP2IX-5 strain after 6h of auxin treatment (Figure 2E and S4A-B). These results indicate that TgAP2IX-5 plays an important role during the early stages of internal budding and is necessary for daughter cell formation.

TgAP2IX-5 is required at a precise time point of the cell cycle.

The *T. gondii* cell cycle has been described precisely and presents a well-organized time line for the division of the subcellular structures of the parasite [14] establishing the following sequence of organelle duplication and segregation: first the centrosome is duplicated and

divided and then the Golgi complex, the apicoplast, the nucleus, the cytoskeleton (e.g. the IMC), the endoplasmic reticulum and eventually the mitochondrion (Figure 3A). To identify the exact timepoint at which TgAP2IX-5 affects daughter parasite formation, a study of the effect of TgAP2IX-5 on organelle duplication and segregation was carried out. During division, the centrosome (outer core) divides first and then the centromere (as well as the inner core centrosome) follows. We measured the ability of the centrosome and centromere to divide within the iKD TgAP2IX-5 strain using TgCentrin1 and TgChromo1 as a centrosome and centromere marker, respectively. For the parental and the iKD TgAP2IX-5 strains, the centrosome to nucleus and centromere to nucleus ratio were recorded after 6 hours of auxin treatment (Figure S5A-C). The recorded ratios of centrosome to nucleus and centromere to nucleus are close to 1 in both the presence and absence of auxin (Figure S5B-C). These results suggest that TgAP2IX-5 does not have a drastic effect on the replication of the centrosome. Similarly, the centromere division is minimally affected, a result that is in line with the multiplication of nuclei observed in the iKD TgAP2IX-5 strain in presence of auxin. However, studying other markers of the centrosome such as TgSFA2 demonstrated that maturation of the centrosome might not be completed (Figure S6A-B).

Since centrosome division remained minimally affected by TgAP2IX-5, a study of the proceeding organelles to divide in the *T. gondii* organelle cell cycle division timeline was carried out. The Golgi complex was labelled in parasites and the ratio of Golgi to nucleus was calculated (Figure 3B). We observed no significant difference between the ratios of Golgi to nucleus in the presence or absence of auxin, therefore suggesting that TgAP2IX-5 depletion does not impact Golgi division and segregation (Figure 3C). We then observed plastid division and segregation (Figure 3B) and measured the plastid to nucleus ratio. This ratio is significantly lower in the iKD TgAP2IX-5 strain in presence of auxin (Figure 3D), suggesting that plastid division is blocked in the mutant. The plastid division is a multistep process where it first

elongates before the completion of scission and segregation [24]. To determine the exact timepoint at which plastid division is affected, the number of parasites with an elongated plastid was recorded in the presence and absence of TgAP2IX-5. We observed a significantly high number of elongated plastid in the absence of TgAP2IX-5 (Figure 3E), suggesting a critical role for TgAP2IX-5 after elongation and before plastid division. This short time frame corresponds to TgAP2IX-5 protein cell cycle dependent expression. As expected, the mitochondria division (the last step during the cell cycle, before cytokinesis) is also affected in the iKD TgAP2IX-5 mutant (Figure S6C), confirming that the blockage during the cell cycle precedes mitochondria division.

TgAP2IX-5 impacts the expression of cell-cycle regulated genes

Since TgAP2IX-5 is a potential transcription factor, we examined the changes in the transcriptome after depletion of the TgAP2IX-5 protein using RNA-seq. Total RNA was purified from tachyzoites of the iKD TgAP2IX-5 strain grown with or without auxin for 6 hours (three biological triplicates). Data analysis using Deseq2 allowed us to identify significant changes in the iKD TgAP2IX-5 transcriptome with an adjusted p-value cutoff of 0.05 and a minimum fold change of 2 (Figure 4A). We identified more than 600 transcripts that were downregulated and around 300 transcripts (Table S2) that were upregulated in the iKD TgAP2IX-5 mutant when treated with auxin (Figure 4A). We examined the cell-cycle expression of the downregulated genes and represented their expression using a heat-map (Figure 4B). We discovered that most of them showed an expression peak during the late S and M phase with a few of them exhibiting a peak during the cytokinesis phase (Figure 4B) while the upregulated genes showed mostly an inverse expression profile showing an expression peak during the G1 phase (Figure S7A). In the list of downregulated transcripts, we were struck by the number of annotated genes corresponding to proteins targeted to the IMC and to the apical complex both structures that are the first to appear when the daughters bud within the mother

cell. To better assess the potential localization of the proteins that correspond to downregulated transcripts, we used a HyperLopit proteomic dataset that predicts with high confidence the localization of proteins in the parasite [25]. We showed that a high proportion of the downregulated transcripts present in the dataset (331 genes) encode proteins predicted to localize to the IMC or to the apical complex (a total of 30% of the downregulated transcripts present in the HyperLopit dataset; Figure S7B). Moreover, these two localizations are overrepresented (16 and 14 %, respectively) when compared to the whole proteome localization (3% for each; 2487 genes, Figure S7C). Based on this dataset, the downregulated genes represent 64 % of the IMC proteome (52/81) and more than 70 % (45/63) of the predicted apical complex proteome. These results suggest that TgAP2IX-5 may act mainly as an activator of genes whose expression shows a cell cycle regulated profile with a peak at the late S and M phases. These genes represent a high proportion of the IMC and apical complex proteome.

By RNA-seq, we were able to identify that TgAP2IX-5 either activates directly or indirectly the expression of genes. In order to identify what promoters are directly targeted by TgAP2IX-5, we carried out a ChIP-seq analysis. Biological duplicates were produced and processed for sequencing (Figure S8A). The MACS2 software was used to identify the significant peaks (p -value < 0.05) that were in intergenic regions close to an annotated gene. This analysis revealed that TgAP2IX-5 directly binds to 696 gene promoters among which key genes are involved in parasite formation (Figure 4C and S8A-D) such as genes encoding proteins targeted to the IMC such as TgIMC1 and TgIMC4 (Figure 4Ci), TgGAPM3 (Figure 4Cii) and TgIMC29 (Figure 4Ciii). Interestingly, we also identified that TgAP2IX-5 was able to bind to the promoters of other ApiAP2 encoding genes (Figure 4Civ and S8C-D). Surprisingly, we found that TgAP2IX-5 was enriched at its own promoter (Figure S8D, boxed) suggesting a possible negative feedback loop for the control of the TgAP2IX-5 transcript expression. We examined the cell cycle expression of the genes whose promoter was targeted by TgAP2IX-5 and found

that a majority of these genes were showing an expression peak during the S and M phase, although a cluster of genes showed a strong expression during C and early G1 phase (Figure S8E). These data confirm the ability of TgAP2IX-5 to act as a bona-fide transcription factor by directly binding to promoters of genes encoding essential proteins for the establishment of the daughter cells.

Since RNA-seq does not enable the identification of the genes that are solely directly controlled by TgAP2IX-5, we overlapped the RNA-seq and ChIP-seq dataset. For that, we identified within the differentially regulated genes list whether they were downregulated or upregulated (as initially identified from RNA-seq), and compared this list with the genes identified to be targeted by TgAP2IX-5 from ChIP-seq analysis using the MACS software. Overall, 117 genes were recorded from the overlap of RNA-seq and ChIP-seq data representing a 17% overlap (Figure 4D). A closer study of the overlap between RNA-seq and ChIP-seq genes identified that 10% of upregulated genes are directly targeted by TgAP2IX-5 whereas 14% of downregulated genes are directly targeted by TgAP2IX-5. We examined the cell cycle regulation of the transcripts directly controlled by TgAP2IX-5 and found that these genes exhibit a cell-cycle regulated expression peak during the late S and early M phases (Figure 4E). These results suggest that TgAP2IX-5 directly controls genes expressed during the S phase and beginning of the M phase. Examples of genes that were found to be directly activated by TgAP2IX-5 included a number of IMC proteins such as TgIMC1, TgIMC4, TgIMC3, TgIMC29 and TgGAPM3 (Table S3). Since TgAP2IX-5 was shown to directly activate genes that are mainly involved in daughter parasite formation, TgIMC29 was myc-tagged within the iKD TgAP2IX-5 strain and we recorded the percentage of TgIMC29 present at site of daughter cell formation. We observed a significant decrease in the TgIMC29 presence at the daughter cell budding site in the absence of TgAP2IX-5 (Figure S9A).

Considering the difference between the RNA-seq and ChIP-seq dataset, we searched the RNA-seq dataset for potential regulators that might be directly regulated by TgAP2IX-5 and therefore may in turn perturb the expression of genes not directly targeted by TgAP2IX-5. Eight ApiAP2 transcription factors were downregulated following the depletion of TgAP2IX-5 as measured by RNA-seq (Figure S9B) and showed an expression peak during the S and M phase (Figure S9B). Among these genes, 4 (TgAP2IV-4, TgAP2III-2, TgAP2XII-9 and TgAP2XII-2) had their promoters directly bound by TgAP2IX-5 (Figure S9B, underlined). Interestingly, much like other genes directly regulated by TgAP2IX-5 (Figure 4E), these genes showed an expression peak during the late S phase (Figure S9B). TgAP2IV-4, a known repressor of developmentally regulated genes, is expressed during the S/M phase [18]. These data suggest that TgAP2IX-5 directly activates other TF during the S phase that may in turn control the late S and M expression program.

Interestingly enough, TgAP2IX-5 which was found to be upregulated in the presence of auxin based on RNA-seq, demonstrated a ChIP-seq peak (Figure S8D) corresponding to its direct targeting by TgAP2IX-5 suggesting that TgAP2IX-5 may be under the direct regulation of a possible negative feedback loop.

Complementation demonstrates TgAP2IX-5 is responsible for the phenotypes observed.

The iKD TgAP2IX-5 mutant was shown to exhibit a multi-nucleated phenotype after depletion of the TgAP2IX-5 protein. The reversibility of this phenotype was studied by generating a complemented strain (iKDc TgAP2IX-5) by inserting a myc-tagged version of the TgAP2IX-5 gene (under the control of its own promoter) into an exogenous locus (*uprt*; Figure S10A). The expression and localization of the exogenous TgAP2IX-5-myc in the complemented strain was verified by immunofluorescence and the percentage of positively labelled parasite with myc-tag was compared to the expression of the endogenous HA-tagged copy. A similar

number of parasites (30 % of the asynchronous parasite population) were shown to express the myc-tagged copy in the complemented strain than the iKD TgAP2IX-5 strain (Figure 5A and S10B). In order to determine whether the multi-nucleated phenotype of iKD TgAP2IX-5 is reversible, the number of nuclei per parasite was recorded in the iKDc TgAP2IX-5 strain in the absence and presence of auxin. We observed that the maximum number of nuclei per parasite did not exceed 2 nuclei per parasite (Figure 5B). These results demonstrated that the multi-nucleated phenotype of iKD TgAP2IX-5 is due to the absence of the TgAP2IX-5 protein. In order to study the effect of reversing the phenotype in iKDc TgAP2IX-5 strain on subcellular components of the cell, Golgi: nucleus and plastid: nucleus ratios were recorded. Calculated ratios of around 1:1 were recorded and we therefore inferred that each parasite contains one Golgi as well as one plastid (Figure 5C-D). These results demonstrate that the TgAP2IX-5 protein was indeed responsible for the phenotypes observed.

TgAP2IX-5 regulates cell cycle pattern flexibility from endodyogeny to endopolygeny

The timing of daughter cell formation is key to define the cell division pattern employed by the parasite at any given time of its life cycle. Since we established that TgAP2IX-5 is the master regulator controlling the production of daughter cells during endodyogeny, we reasoned that controlling the expression of TgAP2IX-5 may be sufficient to switch from one division pattern to another. *T. gondii* undergoes endopolygeny, during its asexual reproduction in the definitive host, where multiple nuclei are formed before a final phase of internal budding. We created a strain of the iKD TgAP2IX-5 mutant expressing a marker of the IMC (TgIMC3-mCherry) to be able to follow the daughter cell formation using live imaging. We treated this strain with auxin to deplete the TgAP2IX-5 protein and obtain parasites that presented around 4 nuclei per parasite (Over-night treatment with auxin). By time-lapse microscopy, we were able to visualize the fate of these parasites after washing auxin out from cell culture media and inducing the re-expression of the TgAP2IX-5 protein. At T₀ we observed enlarged

multinucleated parasites. At T_1 (43 mins after T_0), we started to observe multiple daughter cells emerging from within the initial multinucleated mother parasite labeled with TgIMC3. The emergence of parasites continued throughout T_2 (1.5 hrs after T_0) and T_3 (1.7 hours after T_0). At T_4 (3.9 hours after T_0), we observed individual parasites each separately labelled with TgIMC3 mCherry that had completely emerged from the mother parasite (Figure 6A). After removing auxin from the media, the multinucleated parasites where daughter cell budding was inhibited by the absence of TgAP2IX-5, continued their division in a similar way to endopolygony. Multiple daughter parasites were observed to internally bud within the cytoplasm of the mother cell leading to the release of multiple daughters from an initial multinucleated parasite (Video S1). This forced endopolygony was due to the re-expression of TgAP2IX-5 in these parasites. These data indicate that expression of TgAP2IX-5 controls the entire budding process and that parasites initially depleted from TgAP2IX-5 were still division competent.

To quantify the ability of the parasite to restart division after an initial depletion of TgAP2IX-5, we designed a protocol producing parasites with around 4 nuclei and then observed the effect of the re-expression of TgAP2IX-5 on the number of nuclei per parasite. For that, we counted the number of nuclei per parasite by immunofluorescence at different time points after auxin washout. While this number decreased with longer auxin treatment (Figure 6B), we observed that the number of nuclei per parasite decreases as the duration of auxin washout increases (Figure 6C) indicating that the parasites formed by the “forced” endopolygony are competent for the next cycles of division. However, we noticed a small percentage of parasites with multiple nuclei after overnight auxin washout, indicating that some parasites did not recover from the original depletion of the TgAP2IX-5 protein. In order to study the effect of auxin removal on daughter parasite formation, we recorded the ability of the initial budding capability of the parasite by labelling TgISP1 and TgIMC1 during auxin washout and compared it with

the parasite's budding capability when continuing the auxin treatment. We observed a significant increase in the daughter parasite's budding ability when removing auxin that increased as the duration of auxin washout increased (Figure 6D-6G and S11). To assess if the parasites were able to divide and segregate the apicoplast after depletion and re-expression of TgAP2IX-5, we monitored the fate of the plastid during auxin washout by recording the ratio of plastid to nucleus. While we observed a steady decrease of the number of plastid per nucleus in presence of continuing auxin treatment (Figure 6H), we recorded an increase in the ratio of plastid to nucleus per parasite as the duration of auxin washout increased (Figure 6I) demonstrating that the plastid was competent for replication. These results demonstrate that the timing of TgAP2IX-5 expression is the sole determinant of the creation of daughter cells in the parasite. It may therefore determine the cell division pattern flexibility from endodyogeny to endopolygeny observed in this study.

Discussion

TgAP2IX-5 depletion was found to completely halt the formation of daughter cells (budding cycle) while nuclear division seemed unaffected. When auxin was added at the time of parasite invasion, daughter cell budding was stopped in the first cell cycle, indicating a direct relationship between budding and the expression of TgAP2IX-5. This led to the accumulation of multinucleated parasites without any signs of daughter cell formation. To our knowledge, such a stark phenotype was observed before in a collection of temperature sensitive cell cycle mutants [10], overexpressing a dominant negative version of TgRAb11b [26] and when mutating the specific fibers (SFA2 and 3) that connect the centrosome (outer core) to the forming daughter cells [5]. However, this is the first report demonstrating the importance of transcriptional control in the timing and assembly of daughter cell formation.

After TgAP2IX-5 depletion, the cell cycle stops at a specific timepoint after plastid elongation and before its segregation. This timepoint corresponds to the onset of daughter cell formation. Surprisingly, the nuclear cycle proceeds while the apicoplast remains elongated and is not segregated. This underlines the absence of a checkpoint to ensure proper apicoplast segregation as was observed for other mutants [27].

Flexibility between the nuclear and budding cycle is thought to be controlled in this parasite by the dual core centrosome with the inner core controlling the nuclear cycle and the outer core controlling the budding cycle [9]. A detailed study of the effect of TgAP2IX-5 on the subcellular structures of the parasite revealed that nuclear and bi-partite centrosome division remain mainly unaffected by TgAP2IX-5 depletion. Given the lack of daughter parasite formation observed after TgAP2IX-5 depletion, it is surprising that the outer core centrosome (as represented by TgCentrin1) would remain unaffected. Other components of the outer core, such as the SFA fibers that were shown to be involved in the emergence of daughter cells [5],

but were present at the centrosome after TgAP2IX-5 depletion. Indeed, SFA fiber expression was also unchanged in the mutant as measured by RNA-seq. This indicates that the outer core centrosome functionality is probably intact in the mutant but centrosome activation and maturation is lacking to proceed with the budding cycle. Therefore, it is most likely that depletion of TgAP2IX-5 hinders normal centrosomal activity despite its successful division. The experiments inducing re-expression of TgAP2IX-5 after its depletion further illustrate the undamaged function of the centrosome in absence of the TF, since daughter cell formation restarted after several cycles of unproductive budding. TgAP2IX-5 is therefore the determinant factor for centrosome activation and the control of the budding cycle.

The phenotype observed after TgAP2IX-5 depletion illustrates the independence of the nuclear and budding cycles in this parasite. Using inducible degradation of the TgAP2IX-5 protein, we have established that the tachyzoites are able to divide by endopolygeny *in vitro*. These experiments also underline the ability of the centrosome to duplicate and maintain its functionality in absence of daughter cell formation. This is a key aspect of the parasite centrosome biology that allows to accumulate nuclei and then activate the budding cycle as seen for division patterns such as endopolygeny or schizogony. Although tachyzoites divide by endodyogeny, they retained this ability. This simple mechanism of control which allows multiple nuclear cycles to happen before cytokinesis is also dependent on a single protein, TgAP2IX-5. The presence of TgAP2IX-5 during asexual division in the intermediate host (endodyogeny) or asexual division in the definitive host [28] (endopolygeny) may indicate that the same mechanisms are shared for both division patterns, although global expression profiles are profoundly different. Regulation of the timing of expression of TgAP2IX-5 may be sufficient to switch from one division pattern to another. The molecular mechanisms that count the rounds of DNA synthesis and provide the proper timing for parasite budding may be linked to the proteins that activate the expression of TgAP2IX-5.

We have established that TgAP2IX-5 controls the timing of activation of the centrosome and therefore creation of daughter cells. However, the molecular mechanisms leading to centrosome activation remain unknown. This key event permits the production of daughter cells at the right timing irrespective of the division pattern used. We reasoned that TgAP2IX-5 may directly control the expression of the proteins in charge of centrosome activation. Although expression of the SFA fibers or other known centrosome markers were unaffected in the mutant, we noticed that the expression of a key centrosomal protein, TgCep530, was directly under the control of TgAP2IX-5 (downregulated in RNA-seq and its promoter bound in ChIP-seq). This protein was shown to be targeted to a centrosomal region situated between the inner and outer core [29]. It is essential for the coordination of the nuclear and budding cycle although budding seemed to occur [29]. However, its depletion leads to the accumulation of outer core centrosome [29], a phenotype that is not observed with TgAP2IX-5 expression. This protein may therefore have other functions in the maturation or activation of the outer core centrosome that were not identified previously. Another possibility leading to lack of centrosome activation is a plausible downstream effect of non-transcriptional origin, targeting either a kinase or phosphatase with an important role in the centrosome activation cascade. Key serine/threonine kinases such as MAPK-like protein kinases have been identified within *T. gondii* and have been shown to ensure proper formation of new daughter parasites [9–11]. We found that expression of kinases and phosphatases were downregulated after TgAP2IX-5 depletion, but in our ChIP-seq analysis, TgAP2IX-5 was not found to bind their promoters. One obvious candidate, that is directly regulated by TgAP2IX-5, was the TgCDC48AP protein but it was shown to be involved in apicoplast protein import [30]. TgAP2IX-5 directly activates the expression of several proteins of unidentified function in *T. gondii*; these hypothetical proteins may serve as direct centrosome activators.

We have also established that TgAP2IX-5 directly activates key components of the daughter cell scaffold. In particular, it regulates the expression of components to be targeted early to the forming daughter buds, such as TgISP1 [31], TgIMC1, TgIMC3, TgIMC4 and TgIMC10 [32]. Apical cap component, such as TgAC2 and TgAC7 may also be loaded early on the forming buds. Similarly, TgGAPM3 expression is directly dependent on TgAP2IX-5 and its invalidation provokes IMC collapse [33]. Another example is the TgIMC29 protein that has been shown to have an important role in the formation of daughter cells (Bradley P., personal communication). However, TgIMC15, a protein known to be loaded early on the centrosome before reaching the forming buds is not affected by TgAP2IX-5 depletion. TgIMC15 may have a limited role in daughter cell formation or centrosome activation as suggested by the mild phenotype exerted by its mutant [34]. This suggests that TgAP2IX-5 may activate the centrosome but also directly regulates the expression of key components of the daughter cell scaffold that will be needed in a short time frame to proceed with daughter cell formation (Figure 7).

We observed that RNA-seq and ChIP-seq datasets only partially overlapped. We reasoned that indirect effects on gene expression may be identified using RNA-seq even at a short timing after TgAP2IX-5 depletion (6 hours). The cell-cycle expression profile of the genes that are directly controlled by this TF showed that regulated transcripts are expressed during the S phase before the budding occurs. Among these genes, we identified 4 other ApiAP2 transcription factors (TgAP2III-2, TgAP2IV-4, TgAP2XII-2 and TgAP2XII-9) that were directly controlled by TgAP2IX-5. These TF may be responsible for the expression of the transcripts that were identified as downregulated in RNA-seq and that peak during the late S and M phase. Although no data is available for TgAP2III-2, TgAP2XII-2 and TgAP2XII-9, TgAP2IV-4 was shown to be a repressor of the bradyzoite differentiation expression program [18]. The control of the expression of a repressor of differentiation by a TF that also controls

the continuation of cell cycle may provide the missing link between cell cycle and differentiation. It has been shown that the cell cycle is linked to bradyzoite differentiation [35]. In particular, the developmental switch toward the latent bradyzoite is made during S phase and/or mitosis [35]. It seems convenient for the parasite to link the choice of continuing the tachyzoite cell cycle (by starting the budding cycle) with the expression of a repressor of differentiation. Therefore, expression of TgAP2IX-5 may serve as a molecular check point for the choice between proliferation or differentiation. TgAP2IX-5 may act as a licensing factor for this developmental choice at each round of the cell cycle (Figure 7).

We also observed that TgAP2IX-5 may act as a repressor since it was found at the promoter of genes whose transcript was up-regulated after depletion of this protein. Although, the repressor role is limited to a small number of genes, it was striking to see that the TgAP2IX-5 transcript was overexpressed after TgAP2IX-5 depletion. We also found that TgAP2IX-5 was bound to its own promoter indicating that a direct negative feedback loop may be present to limit the expression of TgAP2IX-5. This might explain the short timeframe when TgAP2IX-5 is expressed during the cell cycle since its expression might be self-limiting. In other eukaryotes, TF associate in complex to either activate or repress gene expression [36]. ApiAP2s are known to associate with each other [21] and differential association may impact their activity.

TgAP2IX-5 is therefore an essential regulator during the *T. gondii* tachyzoite cell cycle. TgAP2IX-5 controls the activation of the outer core centrosome to induce the budding cycle. It also controls the expression of key proteins for formation of the daughter cell scaffold, ensuring that the proper continuation of the cell cycle is achieved. TgAP2IX-5 is also a master regulator that controls the expression of the TF that will be further needed for the completion of the budding cycle. It also acts as a licensing factor that ensures that asexual proliferation continues by promoting the inhibition of the differentiation pathway at each round of the cell

cycle. TgAP2IX-5 is therefore a master regulator that controls cell cycle and developmental pathways.

MATERIALS AND METHODS

Parasite tissue culture and manipulation

Toxoplasma gondii tachyzoites were propagated *in vitro* in human foreskin fibroblasts (HFF) using Dulbecco's modified Eagles medium supplemented with 10% fetal calf serum (FCS), 2mM glutamine, and 1% penicillin-streptomycin. Tachyzoites were grown in ventilated tissue culture flasks at 37°C and 5% CO₂. Transgenes were introduced by electroporation into tachyzoites of *T. gondii* strains and stable transformants were selected by culture in the presence of either 25 µg/ml mycophenolic acid (MPA) and 50 µg/ml xanthine, pyrimethamine (2 µM) or FUDR (5 µg/ml). Clonal lines were obtained by limiting dilution. Prior to total RNA, genomic DNA or protein purification, intracellular parasites were purified by sequential syringe passage with 17-gauge and 26-gauge needles and filtration through a 3-µm polycarbonate membrane filter.

Generation of transgenic T. gondii strains

The iKD TgAP2IX-5 line was generated using RH Δku80 Tir1 strain as described previously [37]. To produce Myc-tagged TgSFA2 (TGME49_205670) or TgIMC29 (TGME49_243200) parasite lines, a DNA fragment representing the tag and the selection cassette was amplified using the pLIC-Myc-DHFR plasmid as a template. The PCR product (10µg) and a pSAG1::Cas9-U6 targeting the 3' UTR of the respective genes were transfected in the iKD TgAP2IX-5 strain. The sequences of all primers used in this study are listed in Supplementary Table 1. In order to generate the iKD complementation line, 60 µg of a plasmid containing 3-kb upstream the predicted ATG of the TgAP2IX-5 gene and the full-length c-myc tagged TgAP2IX-5 gene flanked by 2 kb homology fragments for the *uprt* gene was co-transfected

with the pSAG1::Cas9-U6::sgUPRT plasmid in the iKD TgAP2IX-5 strain to ensure insertion into the UPRT locus. The parasites were then selected using 5 μ M 5-fluoro-2'-deoxyuridine (FUdR). To obtain the iKD TgAP2IX-5 strain expressing TgIMC3-mcherry, the iKD TgAP2IX-5 strain was transfected by a plasmid expressing TgIMC3-mcherry under the *tubulin* promoter and selected using pyrimethamine.

Growth Assays

For the growth assay, 8×10^4 of parental and iKD TgAP2IX-5 parasites per well of a 24 well-plate were inoculated on HFF cells grown on coverslips for 24 hours in normal media or media treated with 0.5 mM of auxin (IAA/indoleacetic acid). The coverslips were then fixated using 4% paraformaldehyde (PFA). The parasite nuclei were stained with anti-TgEno2 and anti-TgIMC1 antibodies and the number of parasites per vacuole was counted. Three independent experiments were performed. For the plaque assay, two hundred of parental and iKD TgAP2IX-5 parasites were inoculated on HFF cells grown in a 6-well plate for seven days in normal media and media treated with 0.5mM of auxin (IAA/indoleacetic acid). Parasites were fixated and then stained using Crystal Violet.

Organelle Labelling

Parental and iKD TgAP2IX-5 strains were inoculated on HFF cells grown on coverslips in a 24 well-plate for 24 hours. This was then followed by the addition of auxin for 3 hours, 6 hours and 12 hours prior to fixation with 4% PFA. The nucleus was labelled with anti-TgEno2 and the number of nuclei per parasite was counted. For Inner Membrane Complex labelling, parental and iKD TgAP2IX-5 strains were left to grow for 24 hours on HFF grown on coverslips for 24 hours. This was then followed by the addition of auxin for 6 hours. Intracellular parasites were labelled using anti-TgISP1 and anti-TgIMC1. Components of the centrosome were labelled after leaving parental and iKD TgAP2IX-5 strains to grow overnight

followed by auxin treatment for 6 hours and TgCentrin1 and TgChromo1 labelling. Golgi, plastid and mitochondrion were labelled after leaving parental and iKD TgAP2IX-5 strains to grow overnight in auxin with anti-TgCT Sort, anti-TgPlastid and anti-TgTom40, respectively.

Immunofluorescence assays

All immunofluorescence assays were carried out using the similar following protocol. Intracellular parasites were fixated using 4% PFA for 30 minutes. The coverslips were incubated with primary antibodies and then secondary antibodies coupled to Alexa Fluor-488 or to Alexa-Fluor-594. Primary antibodies used for IFAs include: anti-TgEno2, anti-TgISP1 [31], anti-TgIMC1 (a gift from Pr. Ward, U. Vermont), anti-TgCentrin1 (a gift from Pr. Gubbels, Boston College), anti-TgChromo1 [23], anti-TgSortilin (Golgi), anti-TgACP (Plastid), anti-TgTom40 [38] (mitochondrion), anti-HA (Eurogentech) and anti-myc (abcam) antibodies were used at the following dilutions: 1:1000, 1:500, 1:500, 1:500, 1:500, 1:500, 1:500, 1:500, 1:200, respectively. Confocal imaging was performed with a ZEISS LSM880 Confocal Microscope or Apotome Microscope at 63 magnification. All images were processed using Carl Zeiss ZEN software.

Electron Microscopy

HFF monolayer was inoculated with iKD TgAP2IX-5 strain. iKD strain was grown in either normal media or media treated with auxin for 24 hours. Transmission electron microscopy samples were fixed with 1 % glutaraldehyde in 0.1 M sodium cacodylate pH 6.8 buffer, at 4°C overnight. They were post-fixed with 1 % osmium tetroxide and 1.5 % potassium ferricyanide then with 1 % uranyl acetate, both in distilled water at room temperature in the dark, for 1 hour. After washing, samples were dehydrated with increasing ethanol-concentration solutions. Samples were finally infiltrated with epoxy resin and cured at 60°C for 24 hours. Sections of 70-80 nm thickness deposited on formvar-coated grids were observed at 80 kV with a Hitachi

H7500 TEM (Milexia, France), and images were acquired with a 1 Mpixel digital camera from AMT (Milexia, France).

Western Blotting

Total protein extracts of 2×10^6 of parental and iKD TgAP2IX-5 parasites grown for 24 hours in either normal media or media treated with auxin were resuspended in 1X SDS buffer. The protein samples were then fractionated on a 6% SDS-polyacrylamide electrophoresis gel and then transferred onto a nitrocellulose membrane. Chemiluminescent detection of bands was carried out by using Super Signal West Femto Maximum Sensitivity Substrate.

Live imaging

The transgenic parasite line iKD TgAP2IX-5 expressing TgIMC3- mCherry was directly inoculated on HFF monolayers grown in an 8 well-chamber. The parasites were left to grow for 7 hours before adding 0.5mM Auxin for 16 hours. Auxin was washed out from the medium by changing normal cell culture media three times. Fluorescent signals were collected sequentially every 13 mins, with an average of 4 lines, a zoom factor (varying between 2 and 4) and resulting in images that were 512x512 pixels in size, and 8 bits in resolution (256 gray levels). The images were treated with ImageJ (NIH). Z-stack acquisitions enabled to visualize the 3D localization of fluorescent signals. Movies were created at a rate of 2 frames per second.

TgAP2IX-5 re-expression experiments

Parasites of the iKD TgAP2IX-5 strain were inoculated on HFF cells grown on coverslips in a 24-well plate for 16 hours in the presence of auxin. Auxin was washed out and parasites were left to grow in auxin-free medium for different durations of time for 3 hours, 6 hours, and 12 hours before fixation with 4% PFA. Parasite nuclei were labelled with TgEno2 and the number of nuclei per parasite were counted. In similar experiments, the parasite's inner membrane complex (IMC) was labelled with TgISP1 and TgIMC1 and the percentage of daughter parasite

formation was measured. In a third comparable experiment, plastid was labelled using anti-TgACP and the ratio of plastid to nuclei was measured. Three independent experiments were performed for each experiment.

RNA sample preparation and extraction

RNA samples were prepared by infecting T175 flasks containing HFF cells monolayer with iKD TgAP2IX-5 parasite for 24 hours in either normal media or media containing auxin. T175 flasks containing intracellular parasite grown in normal media were treated with auxin for 6 hours before sample collection and addition of Trizol (Invitrogen). RNA was extracted as per manufacturer instruction. This was then followed by genomic DNA removal and cleaning using the RNase-free DNase I Amplification Grade Kit (Sigma). All RNA samples were assessed for quality using an Agilent 2100 Bioanalyzer. RNA samples with an integrity score greater than or equal to 8 were included in the RNA library preparation. Triplicate (biological replicate) were produced for each conditions.

RNA library preparation

The TruSeq Stranded mRNA Sample Preparation kit (Illumina) was used to prepare the RNA libraries according to the manufacturer's protocol. Library validation was carried out by using DNA high-sensitivity chips passed on an Agilent 2100 Bioanalyzer. Library quantification was carried out by quantitative PCR (12K QuantStudio).

Chromatin Immunoprecipitation and library preparation.

ChIP was performed using a protocol previously described [21]. Briefly, intracellular parasites were grown 40h and fixed for 10 min at room temperature using 1% formaldehyde. DNA was processed by sonication using the Bioruptor device for 10min at 4°C with a 30sec on/off cycle. Protein-DNA complexes were then diluted in IP Dilution Buffer (16.7mM Tris-HCl pH8, 167mM NaCl, 1.2mM EDTA, 0.01% SDS, 1.1% Triton and 0.5mM PMSF) and incubated ON

with IgG Agarose beads (Amersham Biosciences). The next day, beads were washed five times with ChIP wash buffer (50mM Tris-HCl pH8, 250mM NaCl, 1% NP-40, 1% desoxycholic acid and 0.5mM PMSF) and eluted twice in 75 μ L of ChIP elution buffer (50mM NaHCO₃ and 1% SDS). Duplicate immunoprecipitation and input samples (biological replicate) were produced. Purified DNA (1 ng) was used as a template for library preparation using the Nugen Ovation® Ultralow System V2 kit according to the manufacturer's instructions. Libraries were validated using a Fragment Analyzer and quantified by qPCR (ROCHE LightCycler 480).

Sequencing, pre-processing and dataset cleaning.

Clusters were generated on a flow cell with within a cBot using the Cluster Generation Kit (Illumina). Libraries were sequenced as 50 bp-reads on a HiSeq 2500 using the sequence by synthesis technique (Illumina). HiSeq control software and real-time analysis component were used for image analysis. Illumina's conversion software (bcl2fastq 2.17) was used for demultiplexing. Raw sequencing datasets for RNA-seq (110M total reads) and ChIP-seq (28M total reads) were quality-checked with FastQC v0.11.8-0. Sequencing adapters were trimmed with Cutadapt v1.18 [39]. Finally, low-quality bases (LEADING:20, TRAILING:20, SLIDINGWINDOW:4:25) were trimmed and reads shorter than 30bp were filtered out using Trimmomatic v0.38.1 [40]. FastQC was used to quality-check each intermediary dataset and the final cleaned datasets (105M cleaned RNA-seq reads, 23M cleaned ChIP-seq reads).

RNA-seq analysis

Cleaned datasets (2 conditions * 3 biological replicates * 2 technical replicates = 12 datasets) were aligned with HiSAT2 v2.1.0 [41] against the *T. gondii* ME49 genome from ToxoDB-39 [42] (93M aligned reads), and expression for annotated genes was quantified using htseq-count (union mode) from the HTSeq suite v0.9.1. Raw counts from technical replicates were added before performing differential expression analysis between iKD TgAP2IX-5 samples treated

with or without auxin for 6 hours with DESeq2 v1.22.1 using the SARTools framework v1.6.6 [43]. Differentially expressed genes with adjusted p-value below 0.05 and log₂ fold-change above 2 were kept. The dataset is deposited in the GEO database under the accession number GSE150406.

ChIP-seq analysis

Cleaned datasets (Input & IP * 2 biological replicates * 2 technical replicates = 8 datasets) were aligned with Bowtie2 v2.3.4 against the *T. gondii* ME49 genome from ToxoDB-39 [42] (14M aligned reads). Alignments from biological and technical replicates were merged using SAMtools v1.9 and duplicates were identified with Picard MarkDuplicates v2.18.20. ChIP quality and dataset consistency were checked using the deepTools suite v3.1.3 [44]. Fragment size was estimated and peaks were called with MACS2 v2.1.2 [45]. Additional bigwig tracks comparing ChIP with IP were generated with MACS2 bdgcmp. The dataset is deposited in the GEO database under the accession number GSE150406.

Statistical analysis

All data were analyzed with Graph Pad Prism software (San Diego, California, USA). Differences in the means were assessed by Student's *t*-test. In all cases, $P < 0.05$ was considered as significant.

Funding

This work was supported by Centre National de la Recherche Scientifique (CNRS), Institut National de la Santé et de la Recherche Médicale (INSERM), grants from the French National

Research Agency (ANR) [grant number ANR-13-JSV3-0006-01 to MG] and the CPER CTRL Longévité (to Bilille).

Acknowledgements

The authors wish to thank the BioImaging Center Lille for access to instruments and Lille University for access to the high-performance computing resources and the bilille cloud.

BIBLIOGRAPHY

1. Francia ME, Striepen B. Cell division in apicomplexan parasites. *Nat Rev Microbiol*. 2014;12: 125–136. doi:10.1038/nrmicro3184
2. Gubbels M-J, White M, Szatanek T. The cell cycle and *Toxoplasma gondii* cell division: tightly knit or loosely stitched? *Int J Parasitol*. 2008;38: 1343–1358. doi:10.1016/j.ijpara.2008.06.004
3. Chen C-T, Gubbels M-J. Apicomplexan cell cycle flexibility: centrosome controls the clutch. *Trends Parasitol*. 2015;31: 229–230. doi:10.1016/j.pt.2015.04.003
4. Sheffield HG, Melton ML. The fine structure and reproduction of *Toxoplasma gondii*. *J Parasitol*. 1968;54: 209–226.
5. Francia ME, Jordan CN, Patel JD, Sheiner L, Demerly JL, Fellows JD, et al. Cell Division in Apicomplexan Parasites Is Organized by a Homolog of the Striated Rootlet Fiber of Algal Flagella. *PLOS Biol*. 2012;10: e1001444. doi:10.1371/journal.pbio.1001444
6. Escalante AA, Ayala FJ. Evolutionary origin of Plasmodium and other Apicomplexa based on rRNA genes. *Proc Natl Acad Sci U S A*. 1995;92: 5793–5797.
7. Ferguson DJP, Campbell SA, Henriquez FL, Phan L, Mui E, Richards TA, et al. Enzymes of type II fatty acid synthesis and apicoplast differentiation and division in *Eimeria tenella*. *Int J Parasitol*. 2007;37: 33–51. doi:10.1016/j.ijpara.2006.10.003
8. Gubbels M-J, Lehmann M, Muthalagi M, Jerome ME, Brooks CF, Szatanek T, et al. Forward Genetic Analysis of the Apicomplexan Cell Division Cycle in *Toxoplasma gondii*. *PLOS Pathog*. 2008;4: e36. doi:10.1371/journal.ppat.0040036
9. Suvorova ES, Francia M, Striepen B, White MW. A novel bipartite centrosome coordinates the apicomplexan cell cycle. *PLoS Biol*. 2015;13: e1002093. doi:10.1371/journal.pbio.1002093
10. Gubbels M-J, Lehmann M, Muthalagi M, Jerome ME, Brooks CF, Szatanek T, et al. Forward genetic analysis of the apicomplexan cell division cycle in *Toxoplasma gondii*. *PLoS Pathog*. 2008;4: e36. doi:10.1371/journal.ppat.0040036
11. Alvarez CA, Suvorova ES. Checkpoints of apicomplexan cell division identified in *Toxoplasma gondii*. *PLoS Pathog*. 2017;13: e1006483. doi:10.1371/journal.ppat.1006483

12. Chen C-T, Gubbels M-J. The *Toxoplasma gondii* centrosome is the platform for internal daughter budding as revealed by a Nek1 kinase mutant. *J Cell Sci.* 2013;126: 3344–3355. doi:10.1242/jcs.123364
13. Pelletier L, Stern CA, Pypaert M, Sheff D, Ngô HM, Roper N, et al. Golgi biogenesis in *Toxoplasma gondii*. *Nature.* 2002;418: 548–552. doi:10.1038/nature00946
14. Nishi M, Hu K, Murray JM, Roos DS. Organellar dynamics during the cell cycle of *Toxoplasma gondii*. *J Cell Sci.* 2008;121: 1559–1568. doi:10.1242/jcs.021089
15. Behnke MS, Wootton JC, Lehmann MM, Radke JB, Lucas O, Nawas J, et al. Coordinated progression through two subtranscriptomes underlies the tachyzoite cycle of *Toxoplasma gondii*. *PloS One.* 2010;5: e12354. doi:10.1371/journal.pone.0012354
16. Balaji S, Babu MM, Iyer LM, Aravind L. Discovery of the principal specific transcription factors of Apicomplexa and their implication for the evolution of the AP2-integrase DNA binding domains. *Nucleic Acids Res.* 2005;33: 3994–4006.
17. Walker R, Gissot M, Croken MM, Huot L, Hot D, Kim K, et al. The *Toxoplasma* nuclear factor TgAP2XI-4 controls bradyzoite gene expression and cyst formation. *Mol Microbiol.* 2013;87: 641–655. doi:10.1111/mmi.12121
18. Radke JB, Worth D, Hong D, Huang S, Sullivan WJ, Wilson EH, et al. Transcriptional repression by ApiAP2 factors is central to chronic toxoplasmosis. *PLoS Pathog.* 2018;14: e1007035. doi:10.1371/journal.ppat.1007035
19. Hong D-P, Radke JB, White MW. Opposing Transcriptional Mechanisms Regulate *Toxoplasma* Development. *mSphere.* 2017;2. doi:10.1128/mSphere.00347-16
20. Walker R, Gissot M, Huot L, Alayi TD, Hot D, Marot G, et al. *Toxoplasma* transcription factor TgAP2XI-5 regulates the expression of genes involved in parasite virulence and host invasion. *J Biol Chem.* 2013;288: 31127–31138. doi:10.1074/jbc.M113.486589
21. Lesage KM, Huot L, Mouveaux T, Courjol F, Saliou J-M, Gissot M. Cooperative binding of ApiAP2 transcription factors is crucial for the expression of virulence genes in *Toxoplasma gondii*. *Nucleic Acids Res.* 2018;46: 6057–6068. doi:10.1093/nar/gky373
22. Modrzynska K, Pfander C, Chappell L, Yu L, Suarez C, Dundas K, et al. A Knockout Screen of ApiAP2 Genes Reveals Networks of Interacting Transcriptional Regulators Controlling the Plasmodium Life Cycle. *Cell Host Microbe.* 2017;21: 11–22. doi:10.1016/j.chom.2016.12.003
23. Gissot M, Walker R, Delhay S, Huot L, Hot D, Tomavo S. *Toxoplasma gondii* chromodomain protein 1 binds to heterochromatin and colocalises with centromeres and telomeres at the nuclear periphery. *PloS One.* 2012;7: e32671. doi:10.1371/journal.pone.0032671
24. Blanchard JL, Hicks JS. The non-photosynthetic plastid in malarial parasites and other apicomplexans is derived from outside the green plastid lineage. *J Eukaryot Microbiol.* 1999;46: 367–75.
25. Barylyuk K, Koreny L, Ke H, Butterworth S, Crook OM, Lassadi I, et al. A subcellular atlas of *Toxoplasma* reveals the functional context of the proteome. *bioRxiv.* 2020; 2020.04.23.057125. doi:10.1101/2020.04.23.057125

26. Agop-Nersesian C, Egartter S, Langsley G, Foth BJ, Ferguson DJP, Meissner M. Biogenesis of the inner membrane complex is dependent on vesicular transport by the alveolate specific GTPase Rab11B. *PLoS Pathog.* 2010;6: e1001029. doi:10.1371/journal.ppat.1001029
27. Jacot D, Daher W, Soldati-Favre D. Toxoplasma gondii myosin F, an essential motor for centrosomes positioning and apicoplast inheritance. *EMBO J.* 2013;32: 1702–1716. doi:10.1038/emboj.2013.113
28. Ramakrishnan C, Maier S, Walker RA, Rehrauer H, Joekel DE, Winiger RR, et al. An experimental genetically attenuated live vaccine to prevent transmission of Toxoplasma gondii by cats. *Sci Rep.* 2019;9: 1474. doi:10.1038/s41598-018-37671-8
29. Courjol F, Gissot M. A coiled-coil protein is required for coordination of karyokinesis and cytokinesis in Toxoplasma gondii. *Cell Microbiol.* 2018;20: e12832. doi:10.1111/cmi.12832
30. Fellows JD, Cipriano MJ, Agrawal S, Striepen B. A Plastid Protein That Evolved from Ubiquitin and Is Required for Apicoplast Protein Import in Toxoplasma gondii. *mBio.* 2017;8. doi:10.1128/mBio.00950-17
31. Beck JR, Rodriguez-Fernandez IA, Leon JC de, Huynh M-H, Carruthers VB, Morrisette NS, et al. A Novel Family of Toxoplasma IMC Proteins Displays a Hierarchical Organization and Functions in Coordinating Parasite Division. *PLOS Pathog.* 2010;6: e1001094. doi:10.1371/journal.ppat.1001094
32. Anderson-White BR, Ivey FD, Cheng K, Szatanek T, Lorestani A, Beckers CJ, et al. A family of intermediate filament-like proteins is sequentially assembled into the cytoskeleton of Toxoplasma gondii. *Cell Microbiol.* 2011;13: 18–31. doi:10.1111/j.1462-5822.2010.01514.x
33. Harding CR, Egartter S, Gow M, Jiménez-Ruiz E, Ferguson DJP, Meissner M. Gliding Associated Proteins Play Essential Roles during the Formation of the Inner Membrane Complex of Toxoplasma gondii. *PLOS Pathog.* 2016;12: e1005403. doi:10.1371/journal.ppat.1005403
34. Dubey R, Harrison B, Dangoudoubiyam S, Bandini G, Cheng K, Kosber A, et al. Differential Roles for Inner Membrane Complex Proteins across Toxoplasma gondii and Sarcocystis neurona Development. *mSphere.* 2017;2. doi:10.1128/mSphere.00409-17
35. Radke JR, Guerini MN, Jerome M, White MW. A change in the premitotic period of the cell cycle is associated with bradyzoite differentiation in Toxoplasma gondii. *Mol Biochem Parasitol.* 2003;131: 119–127.
36. Nakagawa T, Yoneda M, Higashi M, Ohkuma Y, Ito T. Enhancer function regulated by combinations of transcription factors and cofactors. *Genes Cells.* 2018;23: 808–821. doi:10.1111/gtc.12634
37. Brown KM, Long S, Sibley LD. Conditional Knockdown of Proteins Using Auxin-inducible Degron (AID) Fusions in Toxoplasma gondii. *Bio-Protoc.* 2018;8. doi:10.21769/BioProtoc.2728
38. van Dooren GG, Yeoh LM, Striepen B, McFadden GI. The Import of Proteins into the Mitochondrion of Toxoplasma gondii. *J Biol Chem.* 2016;291: 19335–19350. doi:10.1074/jbc.M116.725069
39. Martin M. Cutadapt removes adapter sequences from high-throughput sequencing reads. *EMBnet.journal.* 2011;17: 10–12. doi:10.14806/ej.17.1.200

40. Bolger AM, Lohse M, Usadel B. Trimmomatic: a flexible trimmer for Illumina sequence data. *Bioinforma Oxf Engl*. 2014;30: 2114–2120. doi:10.1093/bioinformatics/btu170
41. Kim D, Paggi JM, Park C, Bennett C, Salzberg SL. Graph-based genome alignment and genotyping with HISAT2 and HISAT-genotype. *Nat Biotechnol*. 2019;37: 907–915. doi:10.1038/s41587-019-0201-4
42. Gajria B, Bahl A, Brestelli J, Dommer J, Fischer S, Gao X, et al. ToxoDB: an integrated *Toxoplasma gondii* database resource. *Nucleic Acids Res*. 2008;36: D553-556. doi:10.1093/nar/gkm981
43. Varet H, Brillet-Guéguen L, Coppée J-Y, Dillies M-A. SARTools: A DESeq2- and EdgeR-Based R Pipeline for Comprehensive Differential Analysis of RNA-Seq Data. *PloS One*. 2016;11: e0157022. doi:10.1371/journal.pone.0157022
44. Ramírez F, Ryan DP, Grüning B, Bhardwaj V, Kilpert F, Richter AS, et al. deepTools2: a next generation web server for deep-sequencing data analysis. *Nucleic Acids Res*. 2016;44: W160-165. doi:10.1093/nar/gkw257
45. Zhang Y, Liu T, Meyer CA, Eeckhoutte J, Johnson DS, Bernstein BE, et al. Model-based analysis of ChIP-Seq (MACS). *Genome Biol*. 2008;9: R137. doi:10.1186/gb-2008-9-9-r137

Figure Legends

Figure 1. TgAP2IX-5 is a cell-cycle regulated protein. **(A)** Confocal imaging demonstrating the expression of the TgAP2IX-5 protein using anti-HA antibody during the tachyzoite cell cycle. Anti-TgCentrin1, anti-TgChromo1 and anti-TgISP1 were used as cell cycle markers. The schematic cell cycle phase is indicated on the right side of the figure and the scale bar is indicated on the lower right side of each confocal image. **(B)** Schematic representation of the AID system used to degrade the TgAP2IX-5 protein. This system consists of introducing a recognition sequence into the gene of interest, which expresses a protein fused to the recognition sequence and in the presence of Auxin, will be recognized by the TIR1 protein and degraded by the proteasome. This system was used to produce an inducible knock down parasite in which the expression of TgAP2IX-5 can be controlled. **(C)** Western blot of total protein extract from the parental and iKD TgAP2IX-5 strains treated with Auxin for different durations of time validating the AID system. Western blots were probed with anti-HA to detect the presence of TgAP2IX-5 protein (upper panel), anti-TgActin was used as a control for normalization (lower panel).

Figure 2. Characterization of TgAP2IX-5 iKD parasite. **(A)** Growth assay for parental and iKD TgAP2IX-5 strains in the absence and presence of auxin treatment for 24 hours. The number of parasites per vacuole was measured and the average number of parasites is represented within the graph. A Student's t-test was performed, $***P < 0.001$; mean \pm s.d. (n=3). **(B)** Confocal imaging of iKD TgAP2IX-5 labelled with TgEno2 (red) and TgIMC1 (green) in the presence and absence of auxin treatment. DAPI was used to stain the nucleus. Scale bar is indicated at the lower right side of each image. **(C)** Electron microscopy scans demonstrating the structural morphology of the nucleus in iKD TgAP2IX-5 parasite in the absence and presence of auxin. (N) represents the nucleus. Two daughter parasites are formed within each mother parasite in absence of auxin. Multi-nucleated parasites are visible in presence of auxin.

(D) Bar graphs representing nucleus per parasite counts for parental and iKD TgAP2IX-5 strains in the absence and presence of auxin (12h treatment). A Student's t-test was performed comparing mean percentage of multinucleated parasite between the control (Parental in absence of auxin) and iKD TgAP2IX-5 in the presence of auxin, ***P<0.001; mean \pm s.d. (n=3) (E) Bar graph representing the percentage of daughter parasite formation in the absence and presence of 6 hours of auxin treatment using TgIMC1 labelling, A Student's t-test was performed, ***P < 0.001, **P < 0.01; mean \pm s.d. (n=3).

Figure 3. Organelle replication in iKD TgAP2IX-5 throughout the tachyzoite asexual cell cycle. (A) Schematic representation of the chronological order of organellar division throughout a normal *Toxoplasma gondii* cell cycle. Nuclear cycle is indicated in green and budding cycle is indicated in blue. Time-frame of each organelle division is represented by length of representative organelle. (B) Confocal microscopy of iKD TgAP2IX-5 parasite with labelled plastid (red) and Golgi (green) in the presence and absence of overnight auxin treatment. DAPI was used to stain the nucleus. Scale bar is indicated at the lower right side of each image. (C) Bar graph representing the ratio of Golgi: nucleus using the parental and iKD TgAP2IX-5 strains in the absence and presence of overnight auxin treatment. A Student's t-test was performed, ns: P > 0.05; mean \pm s.d. (n=3). (D) Bar graph representing the ratio of plastid to nucleus using the parental and iKD TgAP2IX-5 strains in the absence and presence of overnight auxin treatment. A Student's t-test was performed, ****P < 0.0001; mean \pm s.d. (n=3). (E) Bar graph representing the percentage of parental and iKD TgAP2IX-5 parasites with an elongated plastid in the absence and presence of overnight auxin treatment. A Student's t-test was performed, ****P < 0.0001; mean \pm s.d. (n=3).

Figure 4: TgAP2IX-5 controls the expression of key genes involved in daughter parasite formation. (A) Volcano plot of differentially expressed genes analyzed from RNA-sequencing of TgAP2IX-5 parasites treated with auxin for 6 hours. Downregulated genes are represented

in blue, upregulated genes are represented in red. Statistically non-significant genes are represented in gray. The differential expression analysis (DE) was based on n=3 independent biological experiments. (B) Heat map showing the cell cycle expression of all individual transcripts that are downregulated in the iKD AP2IX-5 strain in the presence of 6 hours of auxin treatment. The cell cycle phases are represented at the bottom as well as the timing when budding occurs. (C) ChIP-seq data representing the direct targeting of TgAP2IX-5 to the promoters of TgIMC4 (i), TgIMC1 (i), TgGAPM3 (ii), TgIMC29 (iii) and TgAP2XII-2 (iv) genes. MACS2 generated tracks are represented together with the annotated genes (top) (D)Venn diagram of overlapping downregulated genes, upregulated genes from RNA-seq and identified promoters of genes directly interacting with TgAP2IX-5. DEseq2 and MACS2 software were used to analyze RNA-seq and ChIP-seq data respectively. (E) Heat map of the cell cycle expression profile for the 89 downregulated genes directly activated by TgAP2IX-5. The cell cycle phases are represented at the bottom.

Figure 5: iKD TgAP2IX-5 complementation. (A) Bar graph representing the expression of complemented TgAP2IX-5 using anti-myc antibody and the expression of endogenous TgAP2IX-5 using the anti-HA antibody. (B) Bar graph representing nucleus per parasite counts of the iKDc TgAP2IX-5 strain in the presence and absence of overnight auxin treatment. A Student's t-test was performed to compare mean percentage of multinucleated parasite in the iKDc TgAP2IX-5 strain (-auxin) and iKDcTgAP2IX-5 strain (+ auxin), ns: $P > 0.05$; mean \pm s.d. (n=3) (C) Bar graph representing Golgi: nucleus ratio in the iKDc AP2IX-5 strain in the presence and absence of overnight auxin treatment. A Student's t-test was performed, ns: $P > 0.05$; mean \pm s.d. (n=3). (D) Bar graph representing the ratio of plastid/nucleus in the iKDc AP2IX-5 strain in the presence and absence of overnight auxin treatment. A Student's t-test was performed; ns: $P > 0.05$; mean \pm s.d. (n=3).

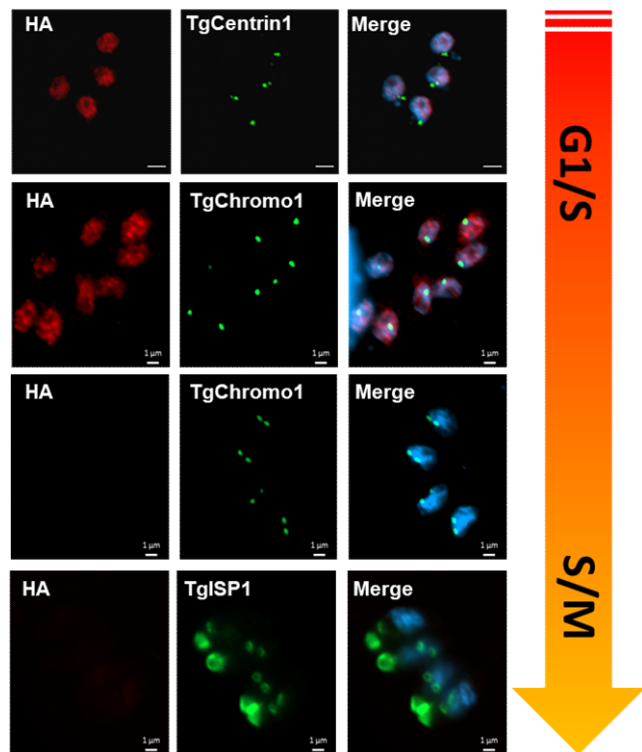
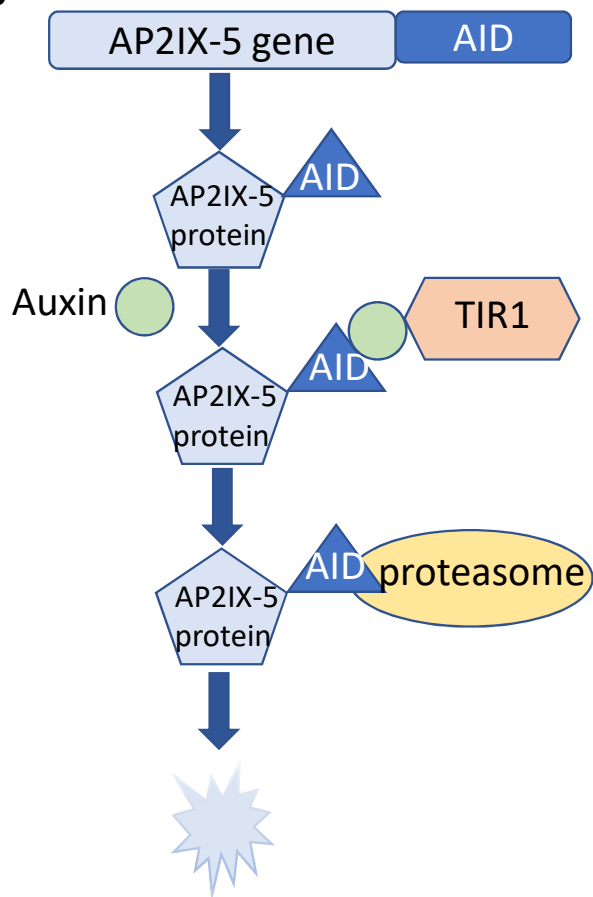
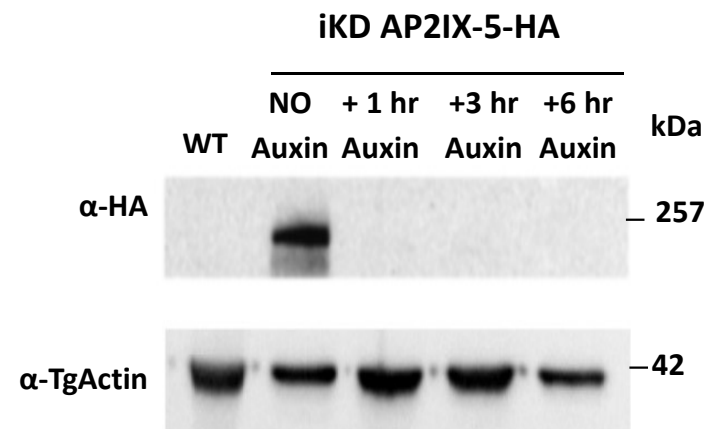
Figure 6: iKD TgAP2IX-5 parasites treated with auxin resume cell division and daughter parasite formation mimicking endopolygony which normally occurs in the felid definitive host after auxin washout (re-expression of TgAP2IX-5). **(A)** Video-microscopy images of iKD TgAP2IX-5 parasites treated with auxin overnight at different time points after auxin washout. T_0 = base line for washout, T_1 = 43 mins after auxin washout, T_2 = 1.5 hrs after auxin washout, T_3 = 1.73 hrs after auxin washout, T_4 = 3.9 hrs after auxin washout. Emergence of parasites is indicated in red arrows throughout the different timepoints. The inner membrane complex of the parasite is labelled with IMC3-mCherry. The budding vacuole is indicated with a red arrow **(B)** Bar graph representing iKD TgAP2IX-5 mutant nucleus per parasite counts treated with auxin for different durations. Timepoint $T_0 = 0$ min is equal to start of auxin wash. A Student's t-test was performed to compare between the mean percentage of multinucleated parasite between the control (Parental -auxin) and iKD TgAP2IX-5 in the presence of auxin, ****P** < 0.01; mean \pm s.d. (n=3). **(C)** Bar graph representing iKD TgAP2IX-5 nucleus per parasite counts during different timepoints of auxin washout treatments; 3 hours, 6 hours and overnight (O/N) washout. A Student's t-test was performed to compare between the mean percentage of multinucleated parasite between the control (Parental Tir1-auxin) and iKD TgAP2IX-5 in the presence of auxin, *****P** < 0.001; mean \pm s.d. (n=3). **(D)** Bar graph representing parasite budding in the iKD TgAP2IX-5 strain during overnight auxin treatment using ISP1 labelling. A Student's t-test was performed, ***P** < 0.05; ****P** < 0.01; mean \pm s.d. (n=3). **(E)** Bar graph representing parasite budding in the iKD TgAP2IX-5 strain using TgISP1 labelling during different timepoints of auxin washout treatments; 3 hours, 6 hours and overnight (O/N) washout. A Student's t-test was performed, ******P** < 0.0001; mean \pm s.d. (n=3). **(F)** Bar graph representing parasite budding in the iKD TgAP2IX-5 strain using TgIMC1 labelling during overnight auxin treatment. A Student's t-test was performed, ns: **P** > 0.05; mean \pm s.d. (n=3). **(G)** Bar graph representing parasite budding in the iKD TgAP2IX-5 strain using TgIMC1

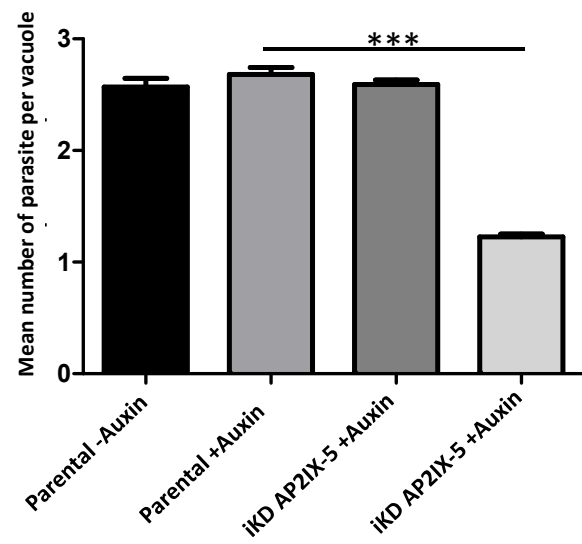
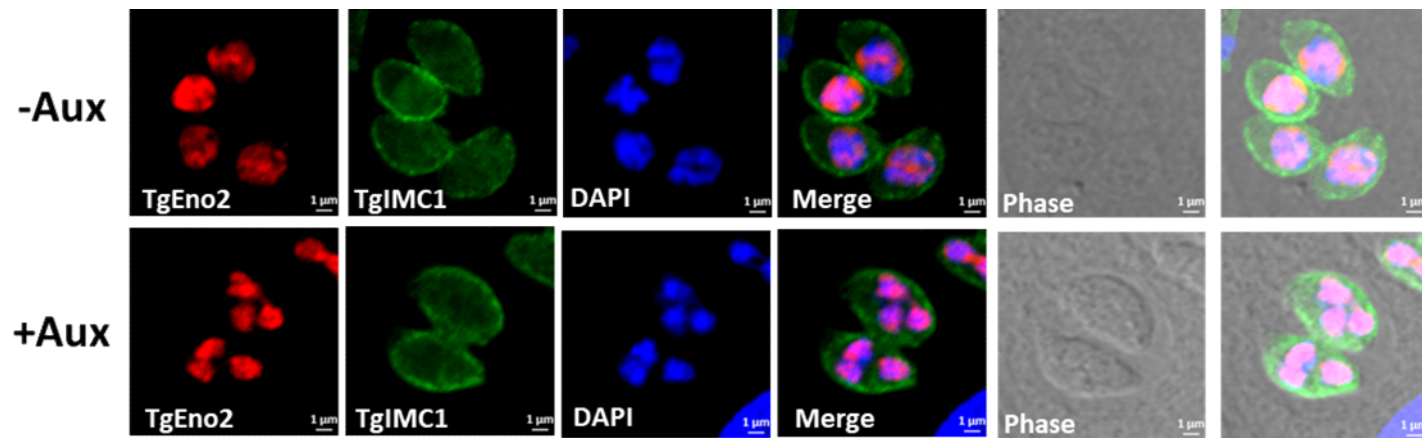
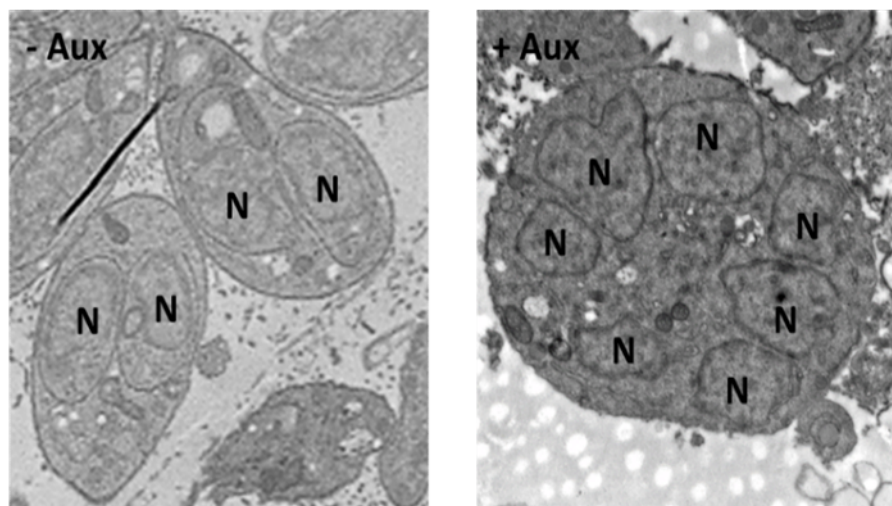
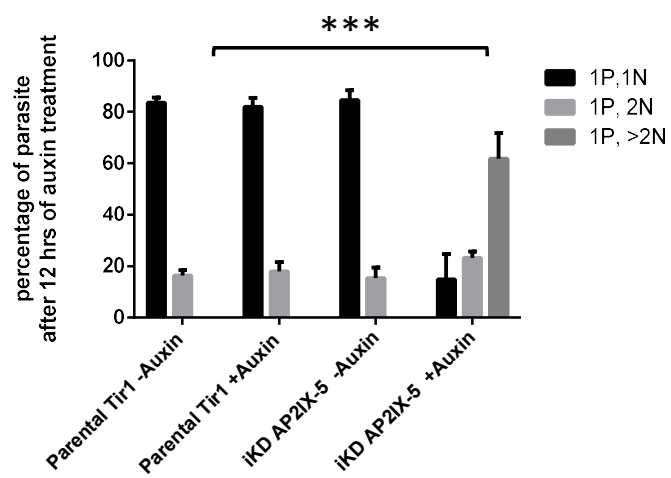
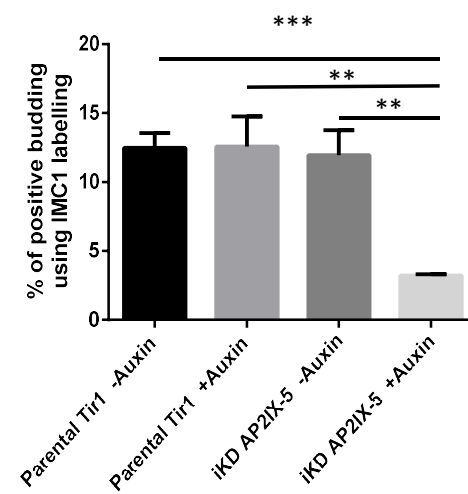
labelling during different time points of auxin washout treatments; 3 hours, 6 hours and overnight (O/N) washout. A Student's t-test was performed, ****P < 0.0001; mean \pm s.d. (n=3).

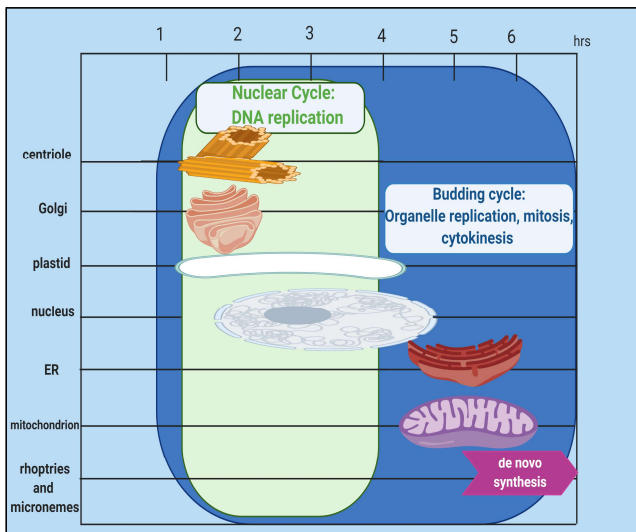
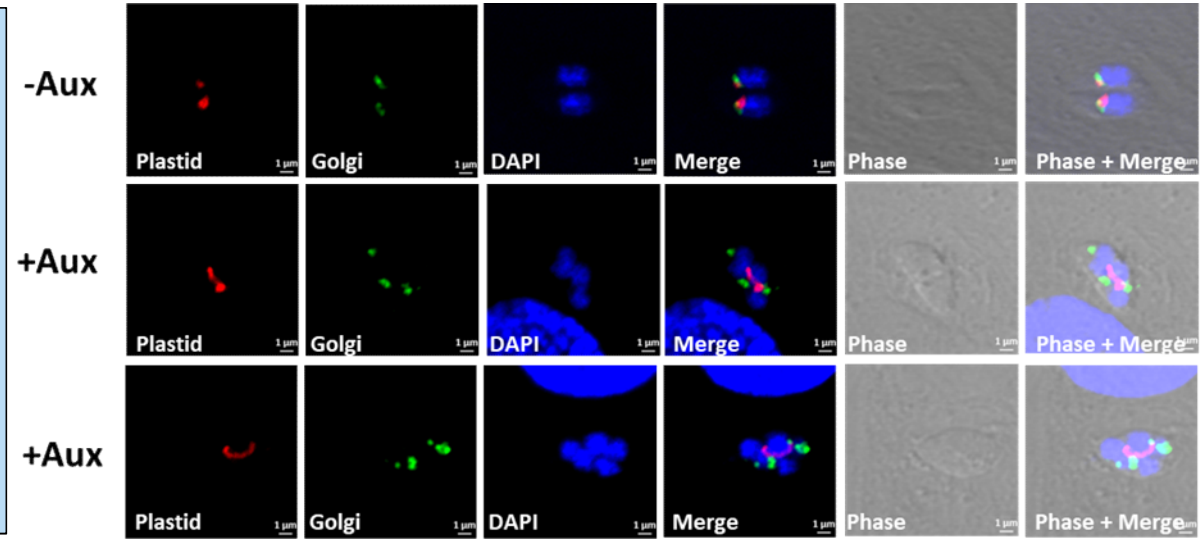
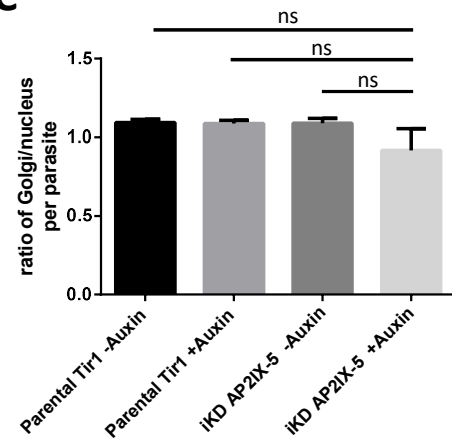
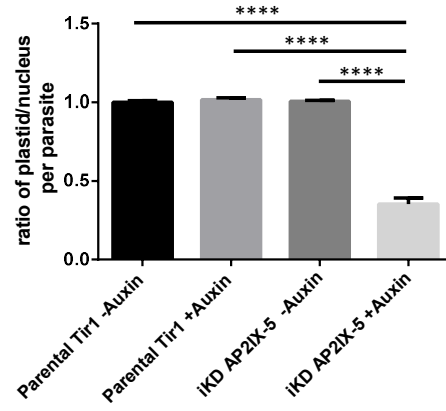
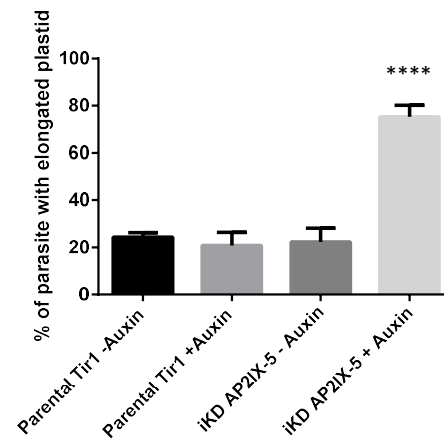
(H) Bar graph representing the ratio of plastid to nucleus in the iKD TgAP2IX-5 strain during overnight auxin treatment. A Student's t-test was performed, **P < 0.01; mean \pm s.d. (n=3). **(I)**

Bar graph representing the ratio of plastid to nucleus in the iKD TgAP2IX-5 strain during different timepoints of auxin washout treatments; 3 hours, 6 hours and overnight (O/N) washout. A Student's t-test was performed, **P < 0.01; *P < 0.05; mean \pm s.d. (n=3).

Figure 7. Schematic representation of the effect of TgAP2IX-5 depletion on daughter cell formation according to the different phases of the cell cycle. Absence of TgAP2IX-5 leads to the blockage of the cell cycle within the G1/S phase. This is associated with the direct targeting and downregulation of key inner membrane complex proteins such as TgISP1, TgIMC1, TgIMC29, TgIMC3, and TgIMC4 as well as other key TFs (TgAP2XII-2, TgAP2XII-9, TgAP2III-2, and TgAP2IV-4). TgAP2IV-4 is a known repressor of differentiation.

A**B****C****Figure 1**

A**B****C****D****E****Figure 2**

A**B****C****D****E****Figure 3**

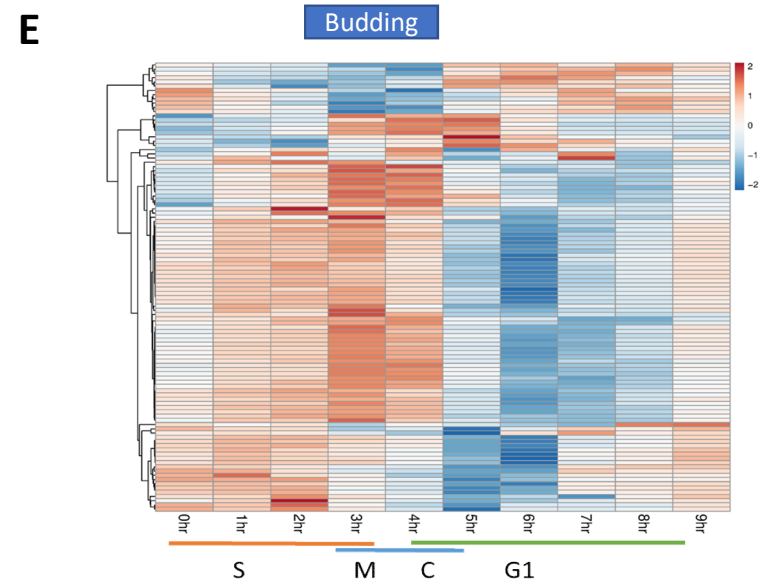
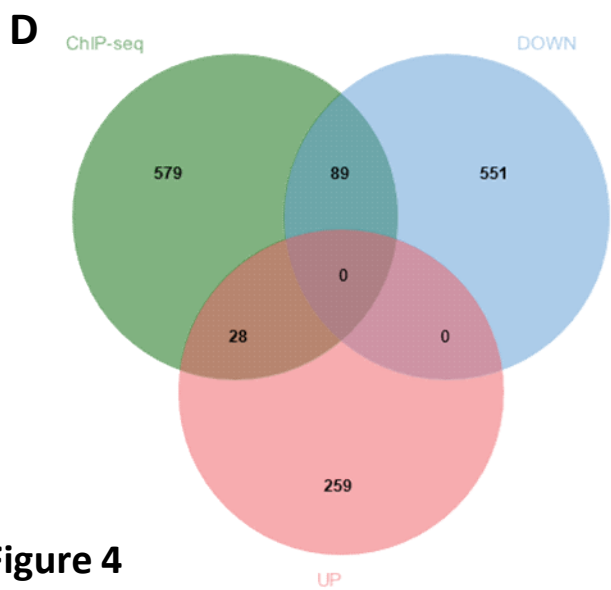
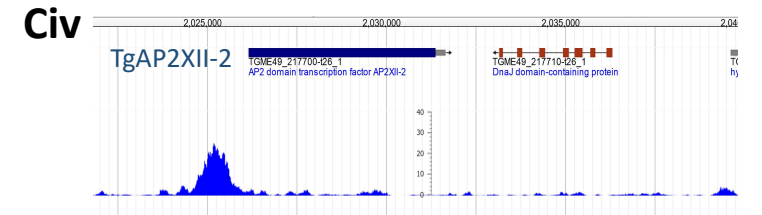
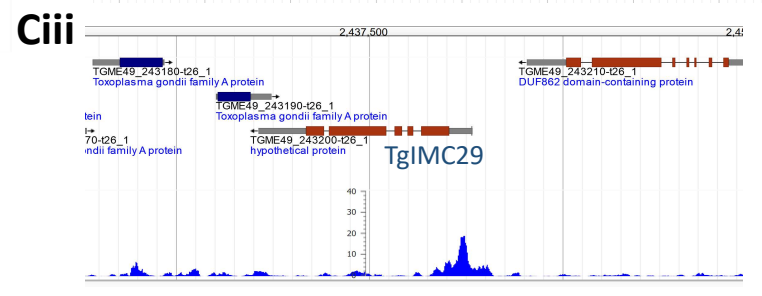
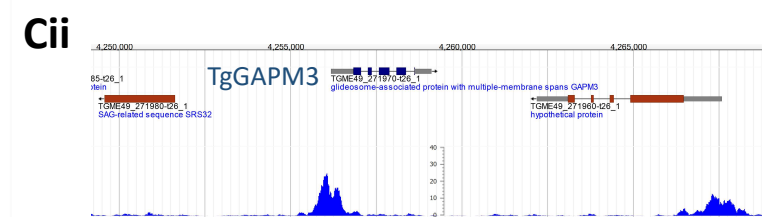
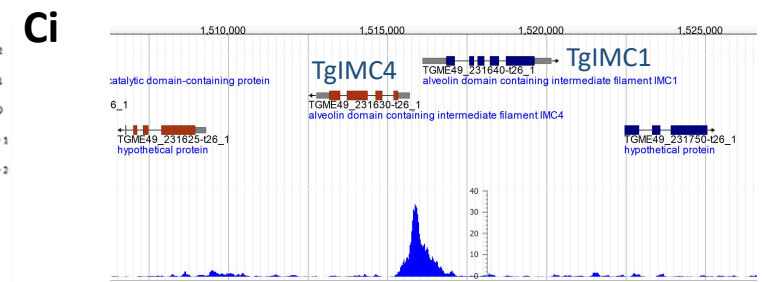
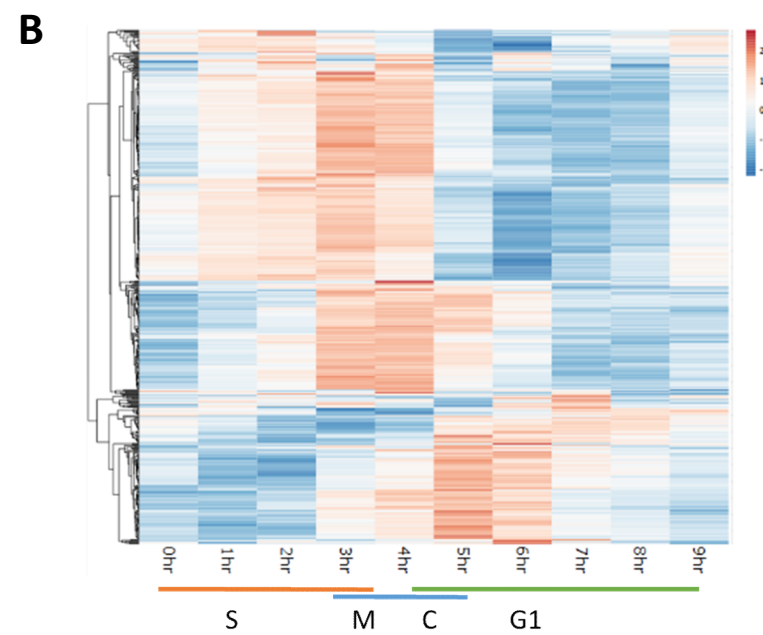
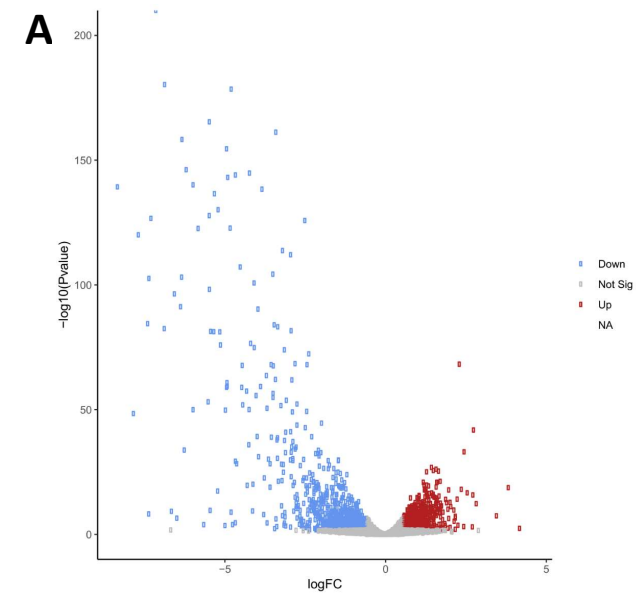
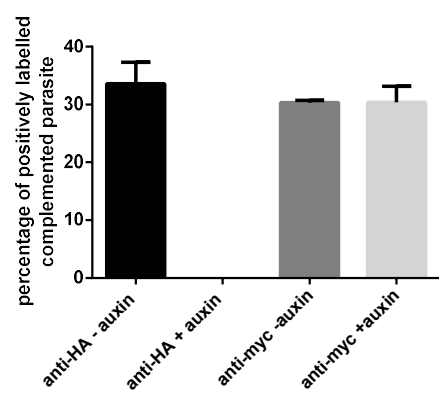
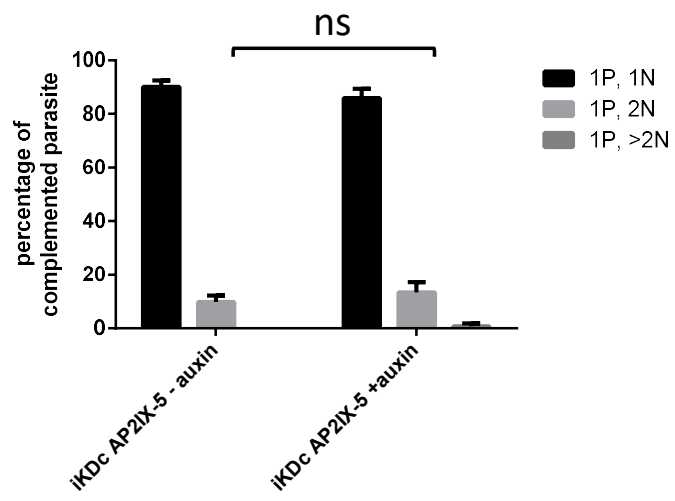
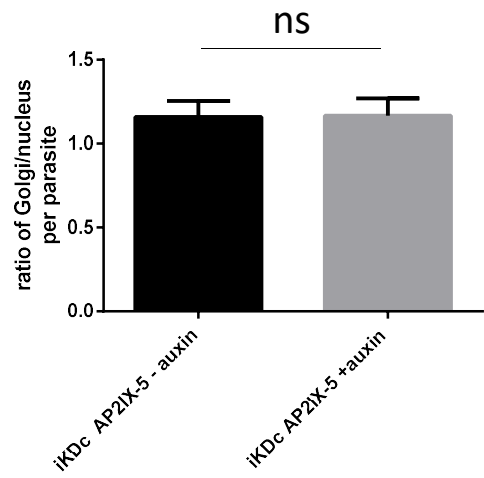
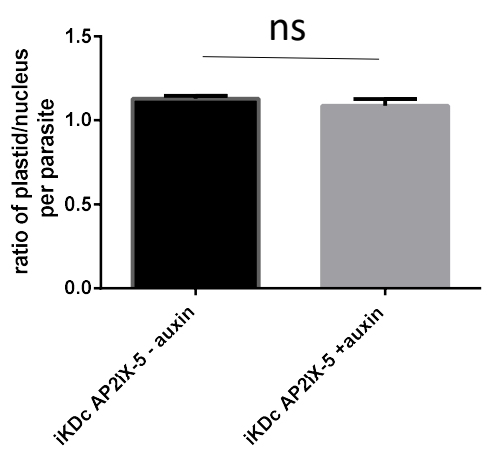


Figure 4

A**B****C****D****Figure 5**

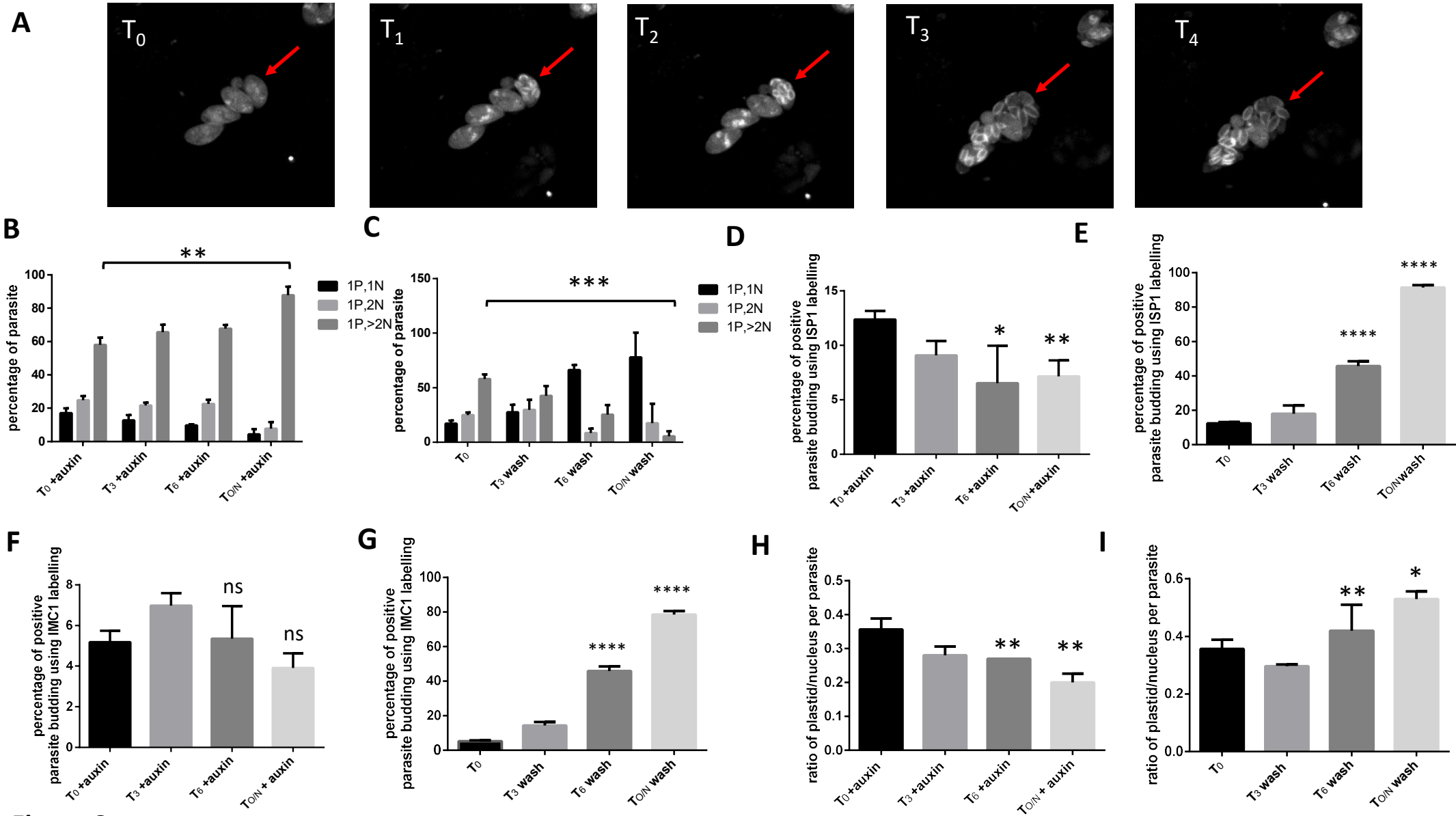


Figure 6

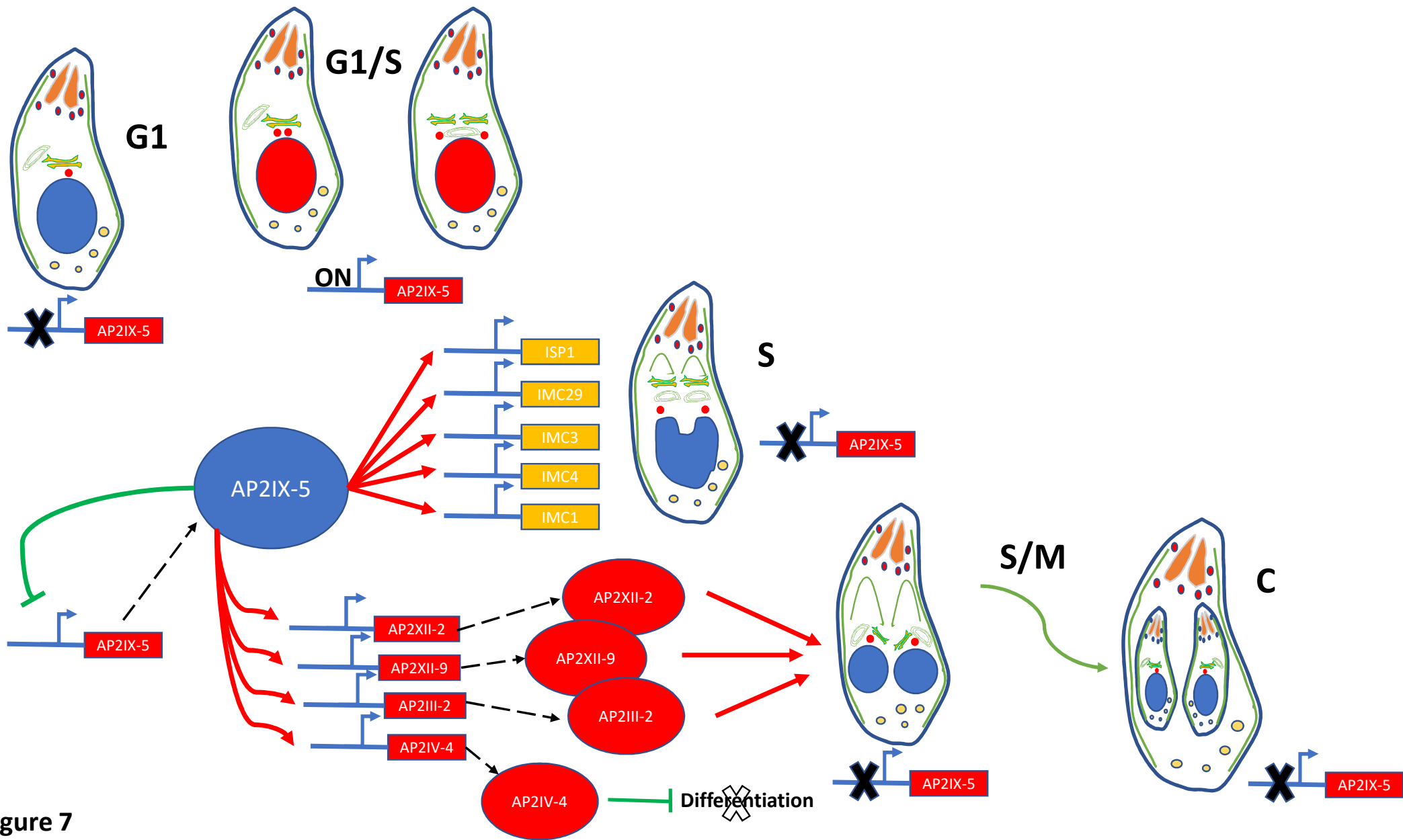


Figure 7